Photo-physical, theoretical and photo-cytotoxic evaluation of a new class of lanthanide (III)–curcumin/diketone complexes for PDT application

Dulal Musib, Mrityunjoy Pal, Md Kausar Raza* and Mithun Roy*

Supporting Information

Table of Content **Page no.**

Methods

1. Reactive oxygen species (ROS) [1]

We have studied singlet oxygen ($^1O_2$) generation via UV-visible (UV-vis) spectrophotometry using 50 μM 1,3-diphenylisobenzofuran (DPBF). DPBF reacted with $^1O_2$ to form an endoperoxide, which decomposed to 1,2-dibenzoylbenzene. The UV-vis spectra of DPBF (λ_{max} 417 nm) were recorded in the presence of the complexes (1-4) (20 μM), exposed to visible light (400–700 nm, 10 J cm^{-2}) for 110 s. A gradual decrease in the absorbance of DPBF indicated the generation of $^1O_2$. We have measured decrease in absorbance of DPBF against the photo-exposure time to monitor the photoactivated generation of singlet oxygen.

2. Singlet oxygen ($^1O_2$) quantum yield determination [2]

Singlet oxygen quantum yield of the complexes (1-4) were determined in DMSO at ambient temperature. Visible light (400-700 nm, 10 J cm^{-2}) was used for the photo-sensitization of the complexes and Rose Bengal (RB). Quantum yields for singlet-oxygen ($^1O_2$), generate by all the complexes were determined by monitoring the photo-oxidation of DPBF. DPBF is a convenient acceptor because it absorbs in a region of dye-transparency and rapidly scavenges singlet oxygen to give colorless products. The quantum yields of singlet-oxygen generation were measured at low dye concentrations (optical density: 0.08– 0.12 at irradiation wavelengths 400-700 nm) to minimize the possibility of singlet-oxygen quenching by the dyes. The photo-oxidation of DPBF was monitored between 10 s to 110 s. The quantum yields of singlet oxygen generation ($\Phi[^1O_2]$) were calculated by a using relative method with optically matched solutions and by comparing the quantum yield of the photo-oxidation of DPBF that was sensitized by the compound of interest to the quantum yield of Rose Bengal (RB) ($\Phi[^1O_2]$= 0.76 in DMSO) as a reference compound according to equation (1),

$$\Phi\Delta_c = \Phi\Delta_{RB} \times (m_c/m_{RB}) \times (F_{RB}/F_c) \quad (1)$$

where c denotes a complex, and RB denotes Rose Bengal. $\Phi\Delta$ is the $^1O_2$ quantum yield, and m is the slope of the plot of DPBF absorbance at 417 nm vs. irradiation time. F is the absorption correction factor, which is given by Equation (2).

$F = 1 - 10^{-OD}$,

(2)

where OD is the optical density at the irradiation wavelength.

3. Computational details [3]

Theoretical calculations for the ligand (L^4) and complexes (1, 3 and 4) were performed using Gaussian 09 version A.02 (Gaussian Inc., USA). The Gaussian 09 input files were prepared using Gauss View 5.0.8. The geometric structures of the complexes and ligand in the ground state were fully optimized at the CAM-B3LYP/GEN level using 6-31G (d, p) basis sets for H, C, N, O, and S atoms. A LANL2DZ basis set was used for La atom in the gas phase. Electronic spectra were generated by performing DFT and TD-DFT calculations to predict absorption in the gas phase and the energies of the corresponding excited states. The chemistry of excited La atom in the gas phase was determined by performing TD-DFT calculations using a CAM-B3LYP/LANL2DZ basis set. Gauss Sum was used to calculate the fractional contributions of various groups to each molecular orbital and the contributions (%) of the metal and ligands to the corresponding HOMOs and LUMOs.

4. MTT assay [4]

The 3-(4,5-dimethylthiazol-2-yl)-2,5-diphenyltetrazolium bromide (MTT) assay was performed for the photocytotoxicity of the complexes (**1**-**4**). In this assay, the mitochondrial dehydrogenases of viable cells cleaved the tetrazolium rings of MTT forming dark purple insoluble formazan crystals that were soluble in DMSO and were quantified from UV-visible spectral measurements. Approximately, 8000 cells of HeLa (cervical cancer cell line), MCF-7 (breast cancer) and MCF-10A cells were plated separately in six different 96 wells culture plate. After 24 h of incubation, various concentrations of complexes 100 to 3.175 μM in 1% DMSO/Dulbecco's modified Eagle's medium (DMEM) were added and pre-incubated for 4 h in the dark. After 4 h of incubation, the media containing compounds were removed and replaced with DPBS buffer which were exposed to visible light (λ = 400-700 nm, light dose = 10 J cm^{-2} 1 h), whereas the other sets were kept in the dark for the same time period using standard protocols. After exposure to light, DPBS was removed and replaced with fresh DMEM media and post-incubation was continued for a 16 h in dark. 4 mg mL^{-1} of MTT (20 μL) solution were added to each well and incubated for an additional 3-4 h. The media was

removed entirely from the wells and then DMSO (200 μL) was added and spectral measurement was taken at 570 nm using TECAN microplate reader. Cytotoxicity of the complexes were measured as the percentage ratio of the absorbance of the treated cells to the untreated controls. The IC_{50} values were determined by nonlinear regression analysis (Graph Pad Prism 6). Data were obtained by using three independent sets of experiments done in triplicate for each concentration.

5. Cellular Localization [4]

By using confocal microscopy, the intracellular localization of the green fluorescent complex **4** in 1% DMSO/DMEM was investigated by confocal microscopy (Zeiss LSM 880 with Airyscan) using an oil immersion lens having a magnification of 63X. About 5 x 10^4 HeLa cells were plated on glass cover slips in 12 well tissue culture plates and incubated at 37°C and 5% CO_2 atmosphere for 24 h. Cells were then treated with the complex **4** (5 μM) for 4 h in dark. Cells were later incubated with PI (1 mg/mL) for 5 min to stain the nucleus. The cover slips were subjected to confocal microscopy after being mounted on slides. Multiple images were recorded, and experiments were done in duplicates to confirm the results.

6. ROS generation [4]

Cellular reactive oxygen species (ROS) was detected by 7'-dichlorofluorescein diacetate (DCFDA) assay. Cellular ROS oxidizes cell permeable DCFDA generating a fluorescent DCF having emission maxima at 528 nm. The percentage population of cells generating ROS was determined by flow cytometry analysis. HeLa cells were incubated with the complexes **1**, **3** and **4** (5 μM) complexes for 4 h and then irradiated with visible light for 40 min (λ = 400-700 nm, light dose = 10 J cm^{-2}). The cells were harvested by trypsinization and a single cell suspension was prepared. The cells were subsequently treated with 1 μM DCFDA (solution prepared with DMSO) in dark for 20 min at room temperature. The distribution of DCFDA stained HeLa cells was obtained by flow cytometry in the FL-1 channel.

7. Cellular Uptake Studies [5]

HeLa cells (about 5 x 10^4) were plated on glass cover slips in 12 well tissue culture plates and incubated at 37°C and 5% CO_2 atmosphere for 24 h. All the three fluorescent complexes **2**, **3** and **4** (5 μM) incubated for 4 h. The cells were then washed once with chilled phosphate buffer saline and analyzed by FACS on an FL2 channel.

8. *Annexin-V- FITC/Propidiumiodide (PI) assay [5]*

About 3 x 10^4 cells were plated in 6 well plates and grown for 24 h. Cells were treated with the control complex **1**(5 μM), photoactive complex **3** and **4** (5 μM) for 4 h. One of the plates was exposed to photo-irradiation (400-700 nm, 1 h) in DPBS with the subsequent addition of fresh

media. The cells were further incubated for 19 h, trypsinized and washed in DPBS twice. The cells were resuspended in 400 µL of 1X binding buffer and 1 µL of annexin V-FITC and 2 µL of PI were added to each cell suspension. These tubes were then incubated at room temperature for 20 min in dark. The fluorescence of the cells was measured immediately with a flow cytometer. Cells that are early in the apoptotic process were stained with the annexin VFITC alone. Live cells showed no staining by either PI or annexin V-FITC. Late apoptotic cells were stained by both PI and annexin V-FITC. The dead cells were only stained by PI.

9. Caspases-3/7 activity and Mitochondrial damage [6]

HeLa cells were seeded in white-walled nontrans parent-bottomed 96-well microculture plates at a density of 3×10^4 cells/well and allowed to incubated overnight to adhere. The cells were then treated with culture medium (negative control, NC), 1% DMSO culture medium (DMSO), 5 µM cisplatin (cis-Pt) or complex **4** (5 µM), respectively. The cells were incubated for 4 h in the dark and divided into two equal parts. The dark group was incubated for additional 30 min and treated with caspase-3/7 activity kit according to the manufacturer's protocol, and the luminescence in RLUs was quantified by an Infinite M200 PRO (TECAN, Swiss). The other groups were exposed to visible light irradiation (400–700 nm, 10 J cm^{-2}), and incubated for additional 30 min in the dark. The caspase-3/7 activity was measured by identical method.

HeLa cells were plated in 6-well culture plates for mitochondrial potential was analysis using the JC-1 dye. Approximately, 3.0 x 10^4 HeLa cells were plated 12-well tissue culture plates and grown for 24 h. The cells were treated with curcumin complex **4** (5 µM, 4 h incubation) with or without 1 h of photo-irradiation (400-700 nm). After 12- 15 hours, the media was removed, and cells were washed with PBS. After staining with the JC-1 dye (25 nM) for 20 min at 37 °C in the dark, the cell suspension was taken into an Eppendorf and centrifuged at 5000 rcf, for 4 min. The fluorescence property of JC-1 dye was used to detect the JC-1 monomer emission at 530 nm (FL1 channel) with aggregates of JC-1 being detected at 580 nm (FL2 channel) through FACS analysis.

References

1. M. K. Raza, K. Mitra, A. Shettar, U. Basu, P. Kondaiah and A. R. Chakravarty, *Dalton Trans.,* 2016, **45**, 13234-13243.
2. D. Musib, M. K. Raza, S. Kundu and M. Roy, *Eur. J. Inorg. Chem.,* 2018, **2018**, 2011-2018.
3. L. R. Devi, M. K. Raza, D. Musib, V. Ramu, J. Devi, M. Roy, *Inorg. Chim. Acta.,* 2019, **500**, 119208.
4. U. Bhattacharyya, B. K. Verma, R. Saha, N. Mukherjee, M. K. Raza, S. Sahoo, P. Kondaiah and A. R. Chakravarty, *ACS Omega,* 2020, **5**, 4282-4292.
5. S. B. Chanu, M. K. Raza, S. Banerjee, P. R. Mina, D. Musib, M. Roy, *J. Chem. Sci*. 2019, **131**, 9.
6. Z. Zhou, J. Liu, T. W. Rees, H. Wang, X. Li, H. Chao, P. J. Stang, *Proc Natl Acad Sci U S A.* 2018, **115**, 5664-5669.

Table S1. Selected bond lengths (Å) and bond angles (˚) obtained from X-ray diffraction data and theoretically optimized structure (using Gaussian 09) of the complex **1**.

Bond Length and Bond angle	Experimental	Theoretical
La-O^1	2.423(3)	2.343
La-O^2	2.416(2)	2.339
La-O^3	2.637(3)	2.577
La-O^4	2.672(3)	2.563
La-O^5	2.696(3)	2.598
La-O^6	2.656(3)	2.623
La-N^1	2.774(3)	2.752
La-N^2	2.688(3)	2.615
La-N^3	2.689(3)	2.663
La-N^4	2.771(2)	2.752
O^1-La-O^2	70.08(9)	72.12
O^1-La-O^3	101.86(9)	104.43
O^1-La-N^3	83.96(9)	84.56
O^1-La-O^8	73.78(9)	77.76
O^2-La-O^3	73.58(8)	76.47
O^2-La-O^5	96.64(8)	98.57
O^2-La-O^6	70.84(8)	76.86
O^2-La-O^8	105.59(8)	109.23
O^2-La-N^1	122.03(8)	124.24
O^2-La-N^2	74.19(8)	76.78
O^3-La-O^5	47.64(8)	48.76
O^3-La-O^6	135.42(8)	138.98
O^3-La-O^8	175.48(8)	177.81
O^3-La-N^1	116.29(7)	119.49
O^5-La-O^6	160.90(9)	161.91
O^5-La-O^8	128.63(9)	127.56
O^5-La-N^1	133.68(8)	135.78
O^6-La-O^8	46.84(8)	49.67
O^6-La-N^1	64.85(8)	66.94

Table S2. Selected UV–Visible energy transitions at the TD-DFT/B3LYP/LanL2DZ level for four La (III) complexes in gas phase.

Complex	Excited state	λ_{cal} (nm), ε_{cal} (M^{-1} cm^{-1}) / eV	Oscillator Strength (f)	λ_{exp}(nm), ε_{exp} (M^{-1} cm^{-1}) / eV	Key transition	Character
1	S_{11}	467.78 (725), (2.6505)	0.0002	429 (230) (2.8901)	HOMO 3 (β) – LUMO 1 (β) (40%)	LMCT
					HOMO 5(β) – LUMO 2 (β) (12%)	LMCT
	S_{15}	376.47 (7034), (3.2933)	0.0017	345 (6210)	HOMO 2 (β) – LUMO (β) (39%)	LMCT
				(3.5937)	HOMO 1 (β) – LUMO 4 (β) (29%)	ILCT
	S_{19}	337.74 (9845), (3.6710)	0.0019	325 (6140)	HOMO 3(β) – LUMO 1 (β) (25%)	ILCT
				(3.8149)		
	S_{23}	296.62 (34522)	0.0743	271 (20710)	HOMO 2 (β) – LUMO 2 (β) (64%)	ILCT
		(4.1799)		(4.5751)		
2	S_{8}	465.52 (982), (2.6633)	0.0005	433 (220), (2.8634)	HOMO 5(β) – LUMO 1 (β) (17%)	LMCT
					HOMO 4(β) – LUMO 1(β) (30%)	LMCT
	S_{13}	434.21 (8486), (2.8554)	0.0089	384 (7540),	HOMO 1(β) – LUMO 2 (β) (21%)	LMCT
				(3.2288)	HOMO 1(β) – LUMO (β) (43%)	ILCT
	S_{21}	386.34 (12356),	0.0101	367 (9610),	HOMO 2(β) – LUMO 1 (β) (32%)	ILCT
		(3.2092)		(3.3783)		
	S_{28}	367.34 (8123), (3.3752)	0.0067	349 (6280),	HOMO (β) – LUMO 2 (β) (36%)	ILCT
				(3.5526)		
	S_{35}	325.76 (29546),	0.068	317 (25700),	HOMO 2(β) – LUMO (β) (12%)	ILCT
		(3.8060)		(3.9112)		
	S_{48}	272.12 (29536),	0.096	283 (21930),	HOMO 3 (β) – LUMO 1 (β) (27%)	ILCT
		(4.5562)		(4.3811)		
3	S_{9}	476.34 (562), (2.6029)	0.0006	441 (320), (2.8114)	HOMO 5(β) – LUMO 2 (β) (29%)	LMCT
	S_{18}	387.46 (15327),	0.0021	377 (10600),	HOMO 4 (β) – LUMO 1(β) (38%)	LMCT
		(3.1999)		(3.2887)	HOMO 4(β) – LUMO 1 (β) (27%)	LMCT/ILCT
	S_{28}	363.57 (16237), (3.4102)	0.0067	354 (13100), (3.5024)	HOMO 2(β) – LUMO 3 (β) (16%)	ILCT
	S_{37}	298.37 (26413), (4.1554)	0.0623	289 (17320), (4.2901)	HOMO 2(β) – LUMO 2 (β) (32%)	ILCT
4	S_{17}	545.56 (5632), (2.2726)	0.0003	536 (1180),	HOMO 2(β) – LUMO 1 (β) (48%)	LMCT
				(2.3131)	HOMO 1 (β) – LUMO 3 (β) (26%)	LMCT
	S_{21}	431.32 (16523),	0.0172	452 (11300),	HOMO 6 (β) – LUMO (β) (29%)	LMCT
		(2.8745)		(2.7430)	HOMO 4 (β) – LUMO 2 (β) (41%)	ILCT
	S_{27}	437.43 (19326), (2.8344)	0.0352	428 (12700), (2.8968)	HOMO 1 (β) – LUMO 1 (β) (29%)	ILCT
	S_{32}	356.78 (598), (3.4751)	0.0006	340 (310), (3.6466)	HOMO 3 (β) – LUMO (β) (29%)	ILCT
	S_{43}	284.59 (19437), (4.3566)	0.0783	271 (16570), (4.5751)	HOMO 2 (β) – LUMO (β) (29%)	ILCT

Table S3: The rate of dissociation of the complexes (1-4) in in 1% DMSO/Dulbecco's modified Eagle's medium (DMEM)	
Complex	Rate constant (h^{-1})
1	2.47×10^{-5}
2	9.3×10^{-5}
3	8.61×10^{-5}
4	2.30×10^{-5}

Table S4. Selected low-lying excited states, dominant Orbital Excitation, orbital character and calculated energies **(**E**)** from TD-DFT Calculations for La**(**III**)** complexes (1, 2, 3 and 4) and ligand (L^4) Calculated at TD-DFT/CAM-B3LYP/631G**(**d,p**)**/LanL2DZ level**.**

Complex	Excited State	Orbital excitation	Character	-E[a] (a.u)
1	T_1	HOMO-1(β)-LUMO-1(β) (62%)	MLCT	2271.68814
	S_1	HOMO (β)-LUMO-2(β) (58%)	MLCT	2271.65623
2	T_1	HOMO-1(β)-LUMO (β) (43%)	MLCT	2618.44165
	S_1	HOMO (β)-LUMO-1(β) (50%)	MLCT	2618.42157
3	T_1	HOMO-1(β)-LUMO (β) (48%)	ILCT	2723.78651
	S_1	HOMO (β)-LUMO-2 (β) (61%)	ILCT/MLCT	2723.77024
4	T_1	HOMO-2(β)-LUMO (β) (57%)	ILCT	2997.60124
	S_1	HOMO(β)-LUMO-1(β) (36%)	MLCT	2997.59012
L^4	T_1	HOMO (β)-LUMO-1 (β) (45%)	ILCT	1263.03742
	S_1	HOMO(β)-LUMO (β) (64%)	ILCT	1263.01264

[a]The energy value corresponds to the absolute energy of the respective states.

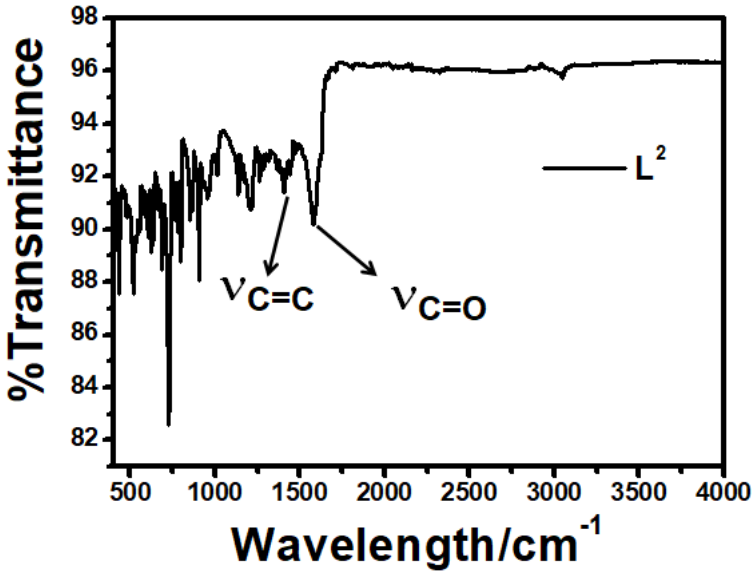

Figure S1: Solid-phase FT-IR Spectra of **L^2** recorded in KBr phase using Perkin-Elmer UATR TWO FT-IR Spectrometer.

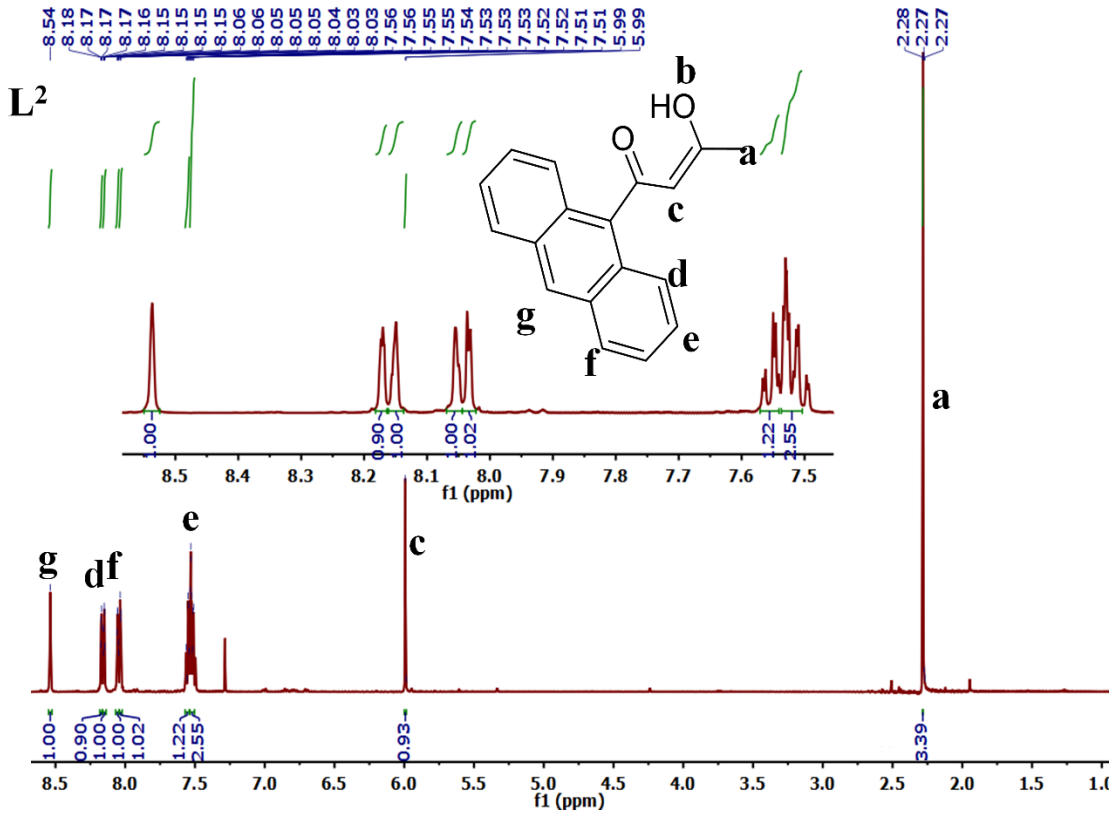

Figure S2: ^{1}H NMR of **L²** recorded in $CDCl_3$ using Bruker Avance 400 (400 MHz) spectrometer.

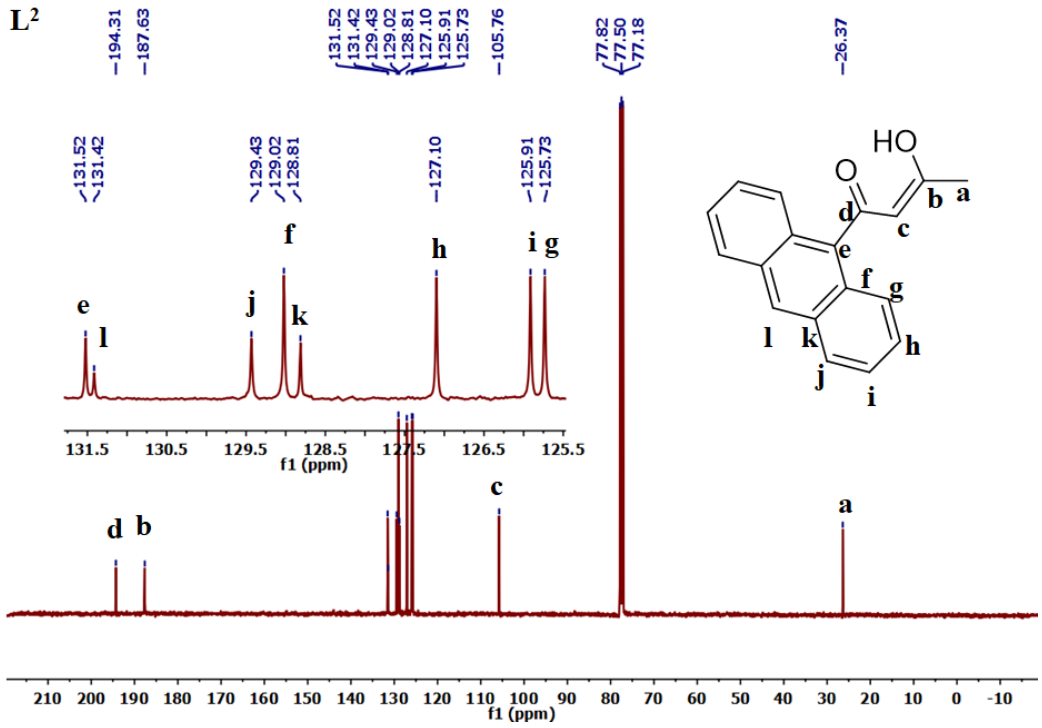

Figure S3: ^{13}C NMR of **L²** recorded in $CDCl_3$ using Bruker Avance 400 (100 MHz) spectrometer.

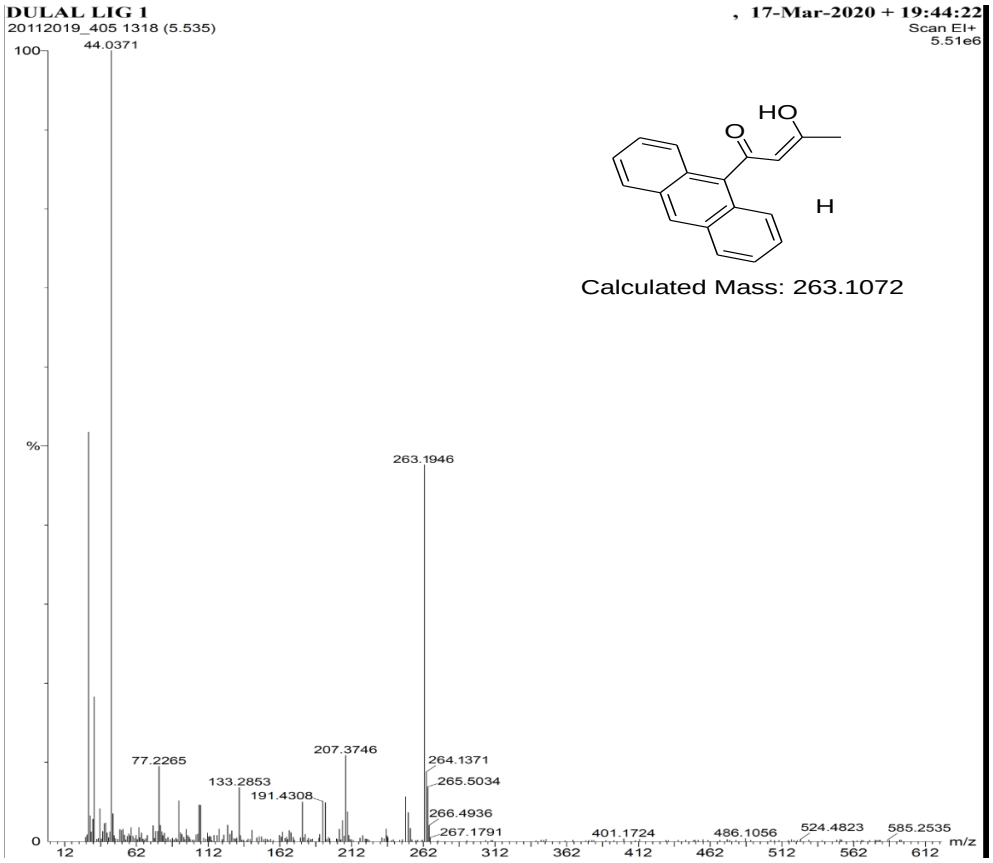

Figure S4: HR-Mass spectra of the $\mathbf{L^2}$ recorded in CH_3OH. The peak at m/z 263.1946 corresponds to the species $[\mathbf{L^2H}]^+$.

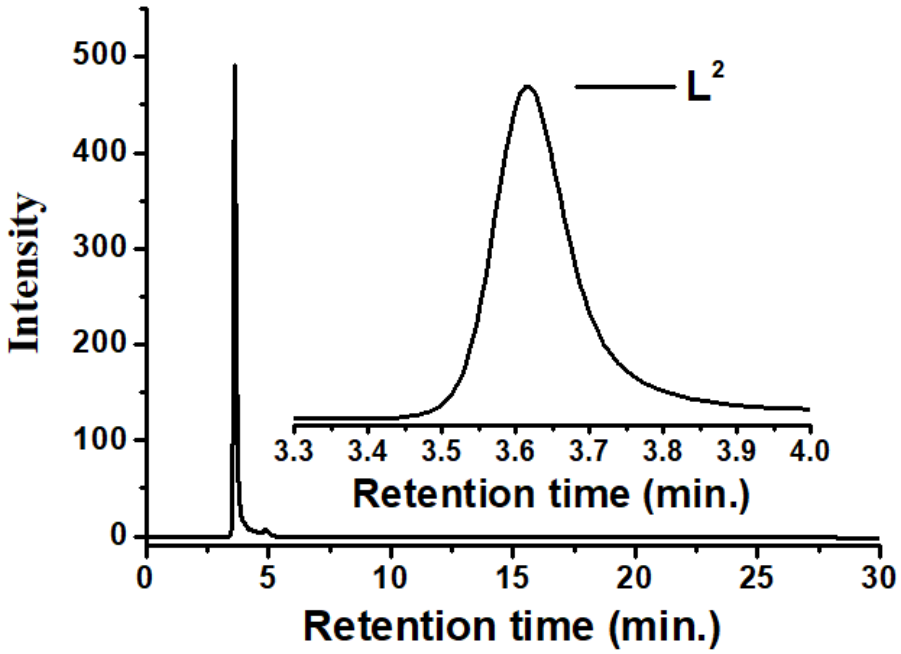

Figure S5: HPLC chromatograms for the ligand ($\mathbf{L^2}$) (Condition: UV = 254nm, flow rate 0.5 ml/min, solvent = H_2O: IPA = 95:5).

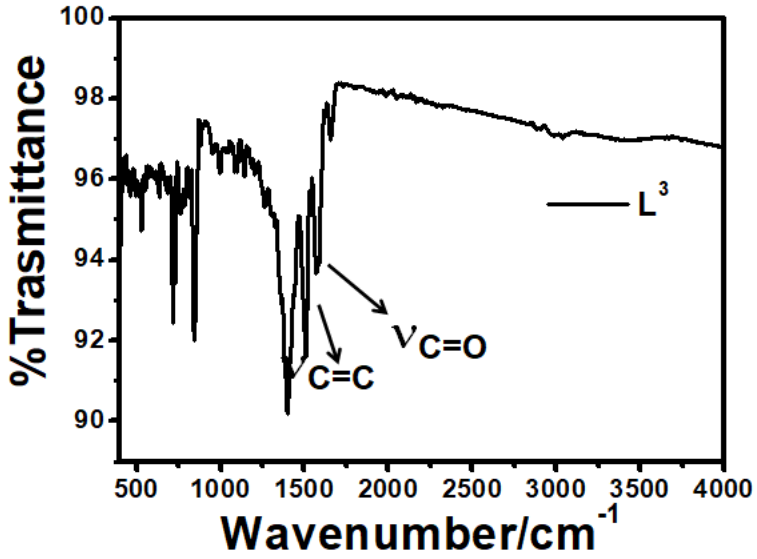

Figure S6: FT-IR Spectra of **L**^{3} recorded in KBr phase using Perkin-Elmer UATR TWO FT-IR Spectrometer.

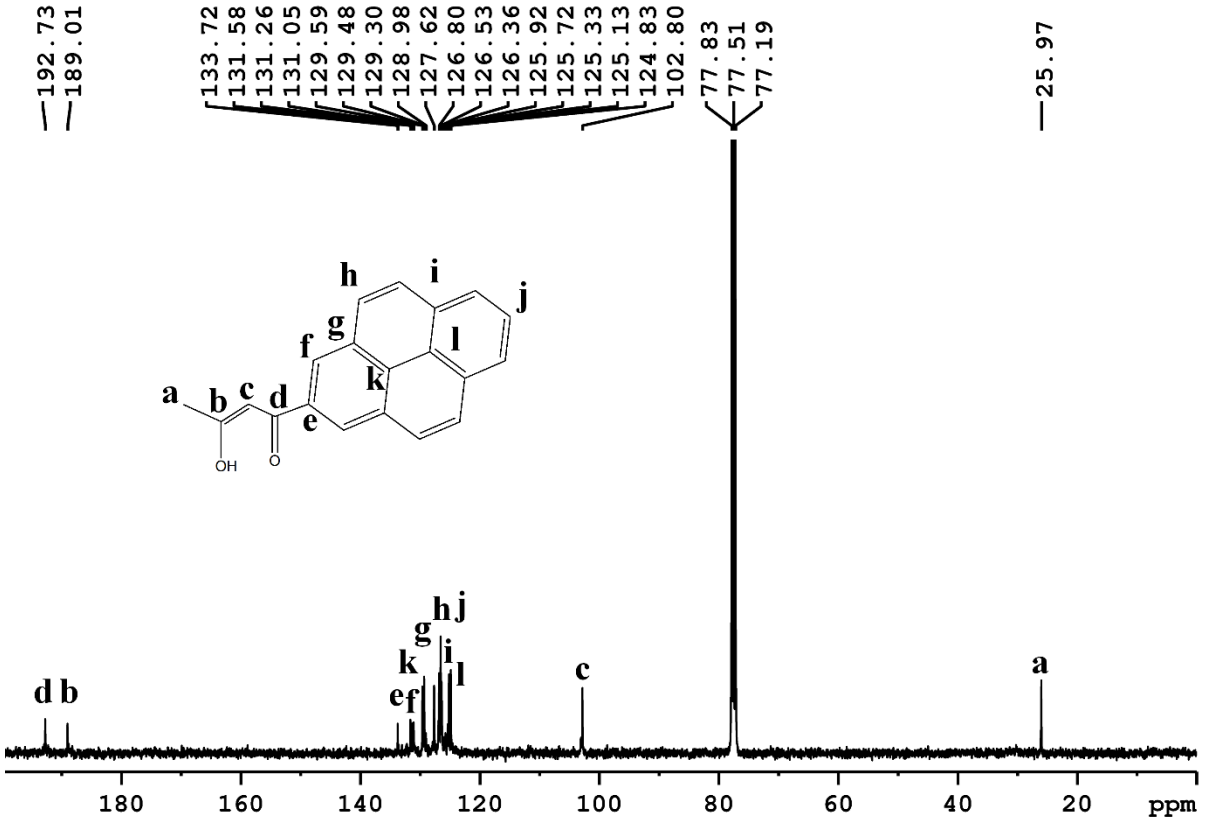

Figure S7: ^{13}C NMR of **L**^{3} recorded in $CDCl_3$ using Bruker Avance 400 (100 MHz) spectrometer.

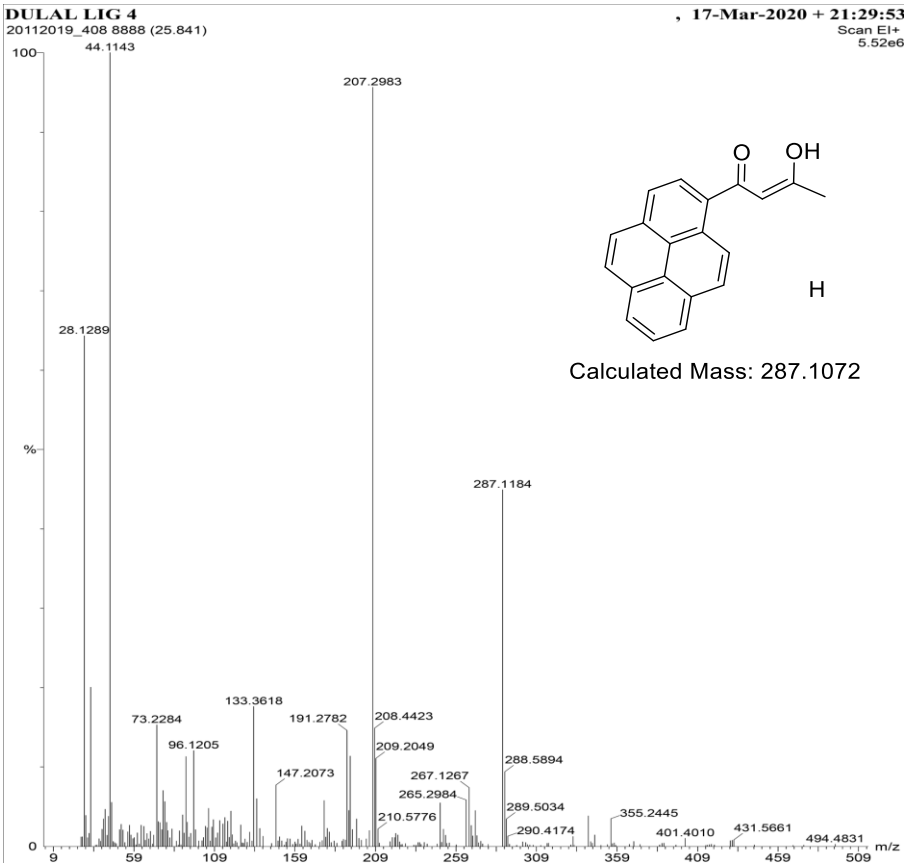

Figure S8: HR-Mass spectra of the $\mathbf{L^3}$ recorded in CH_3OH. The peak at m/z 287.1184 corresponds to the species $[\mathbf{L^3H}]^+$.

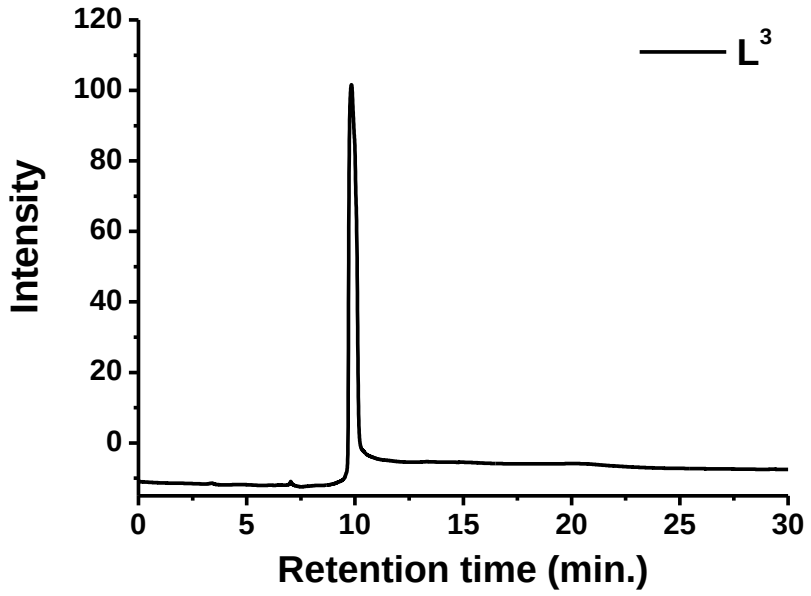

Figure S9: HPLC chromatograms for the ligand ($\mathbf{L^3}$) **(**Condition: UV = 254nm, flow rate 0.5 ml/min, solvent = H_2O: IPA = 95:5).

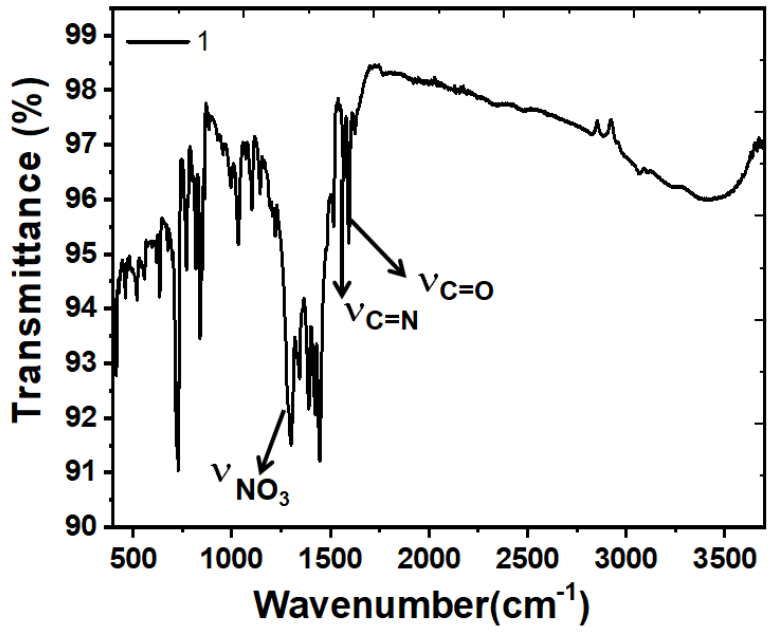

Figure S10: Solid phase FT-IR spectra of the complex **1**.

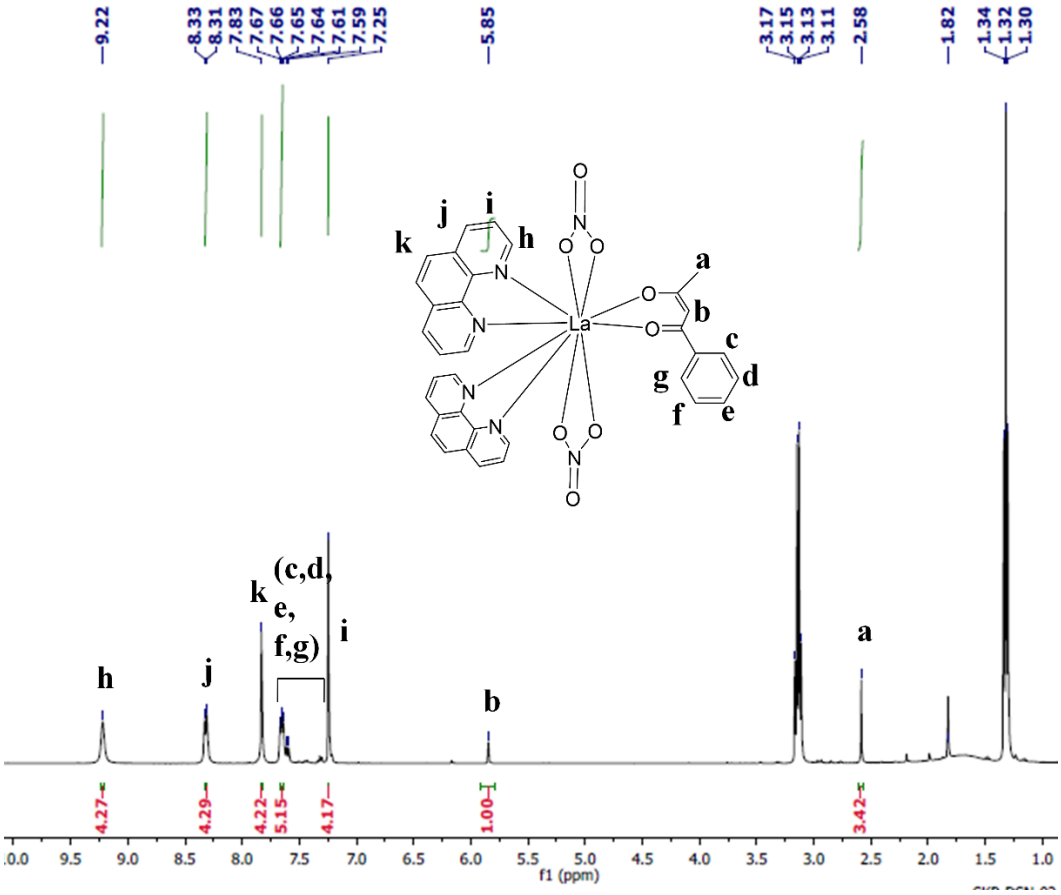

Figure S11: ^{1}H NMR of **1** recorded in $CDCl_3$ using Bruker Avance 400 (400 MHz) spectrometer.

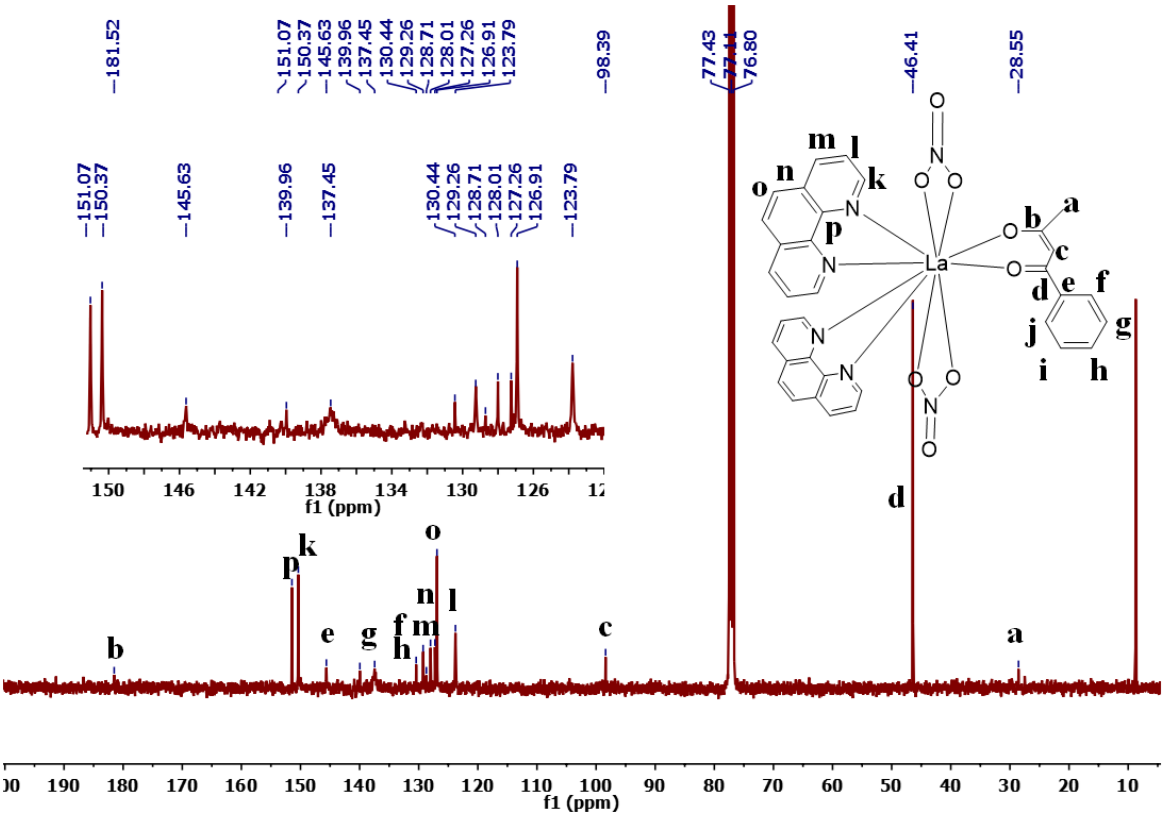

Figure S12: ^{13}C NMR of **1** recorded in $CDCl_3$ Bruker Avance 400 (100 MHz) spectrometer.

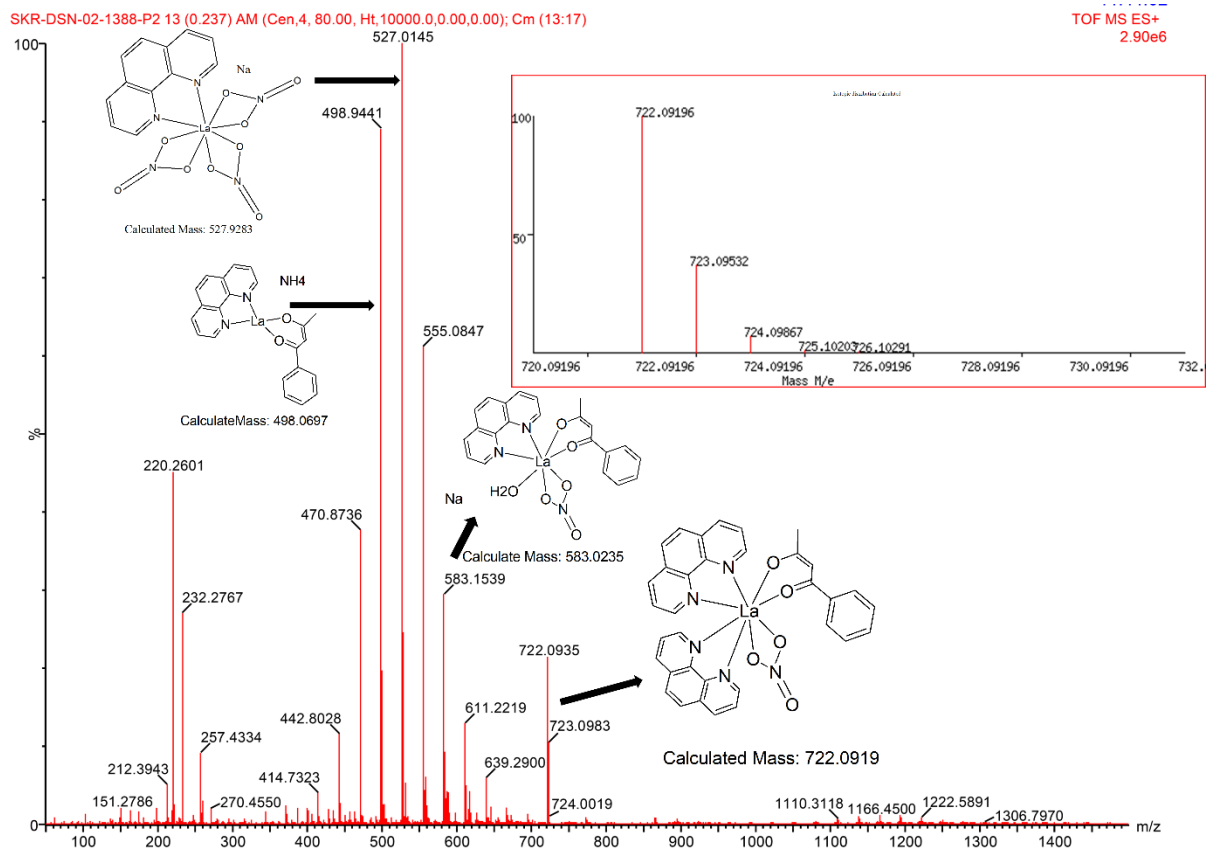

Figure S13: Q-TOF ESI Mass spectra of the **1** recorded in CH_3OH using Bruker Esquire 3000 Plus spectro-photometer (Bruker-Franzen Analytic GmbH, Bremen, Germany). The peak at

m/z 722.0935 corresponds to the species $[M-(NO_3^-)]^+$ and the highest peak 527.0145 corresponds to the species $[Na\{M(NO_3)\}-(L^1)(phen.)]^+$.

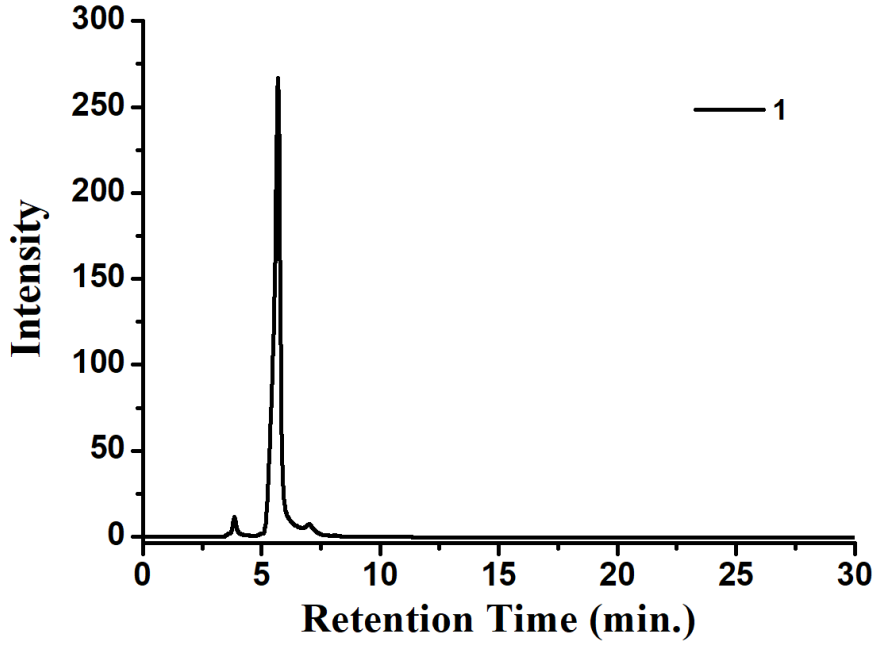

Figure S14: HPLC chromatograms for the complex (**1**) **(**Condition: UV = 254nm, flow rate 0.5 ml/min, solvent = H_2O: IPA = 95:5).

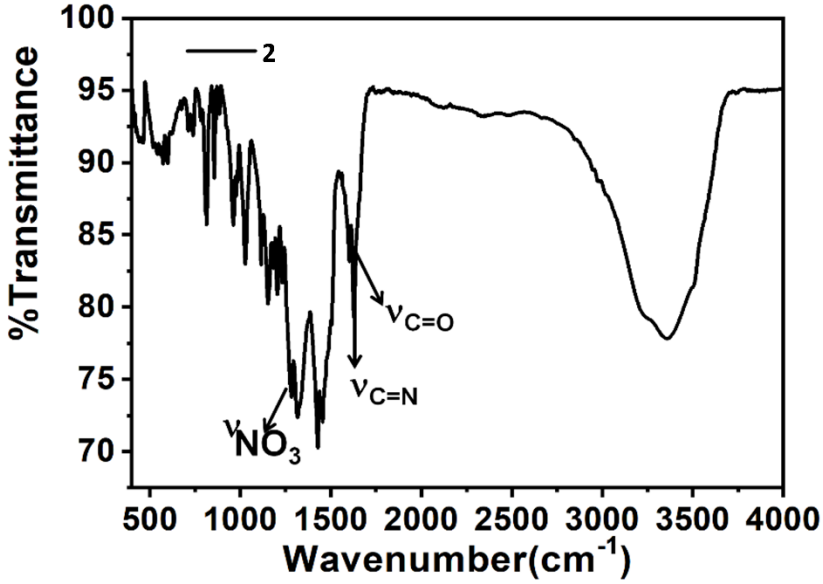

Figure S15: Solid phase FT-IR spectra of the complex **2**.

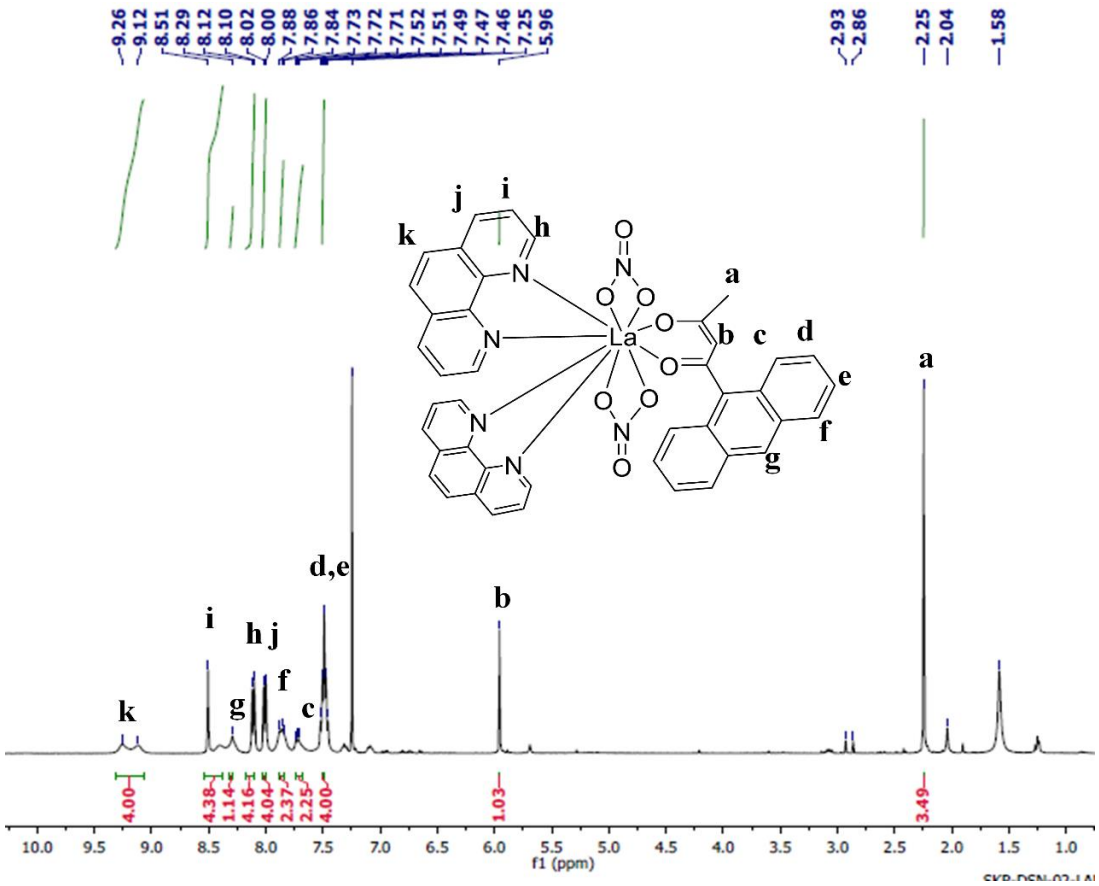

Figure S16: ^{1}H NMR of **2** recorded in $CDCl_3$ using Bruker Avance 400 (400 MHz) spectrometer.

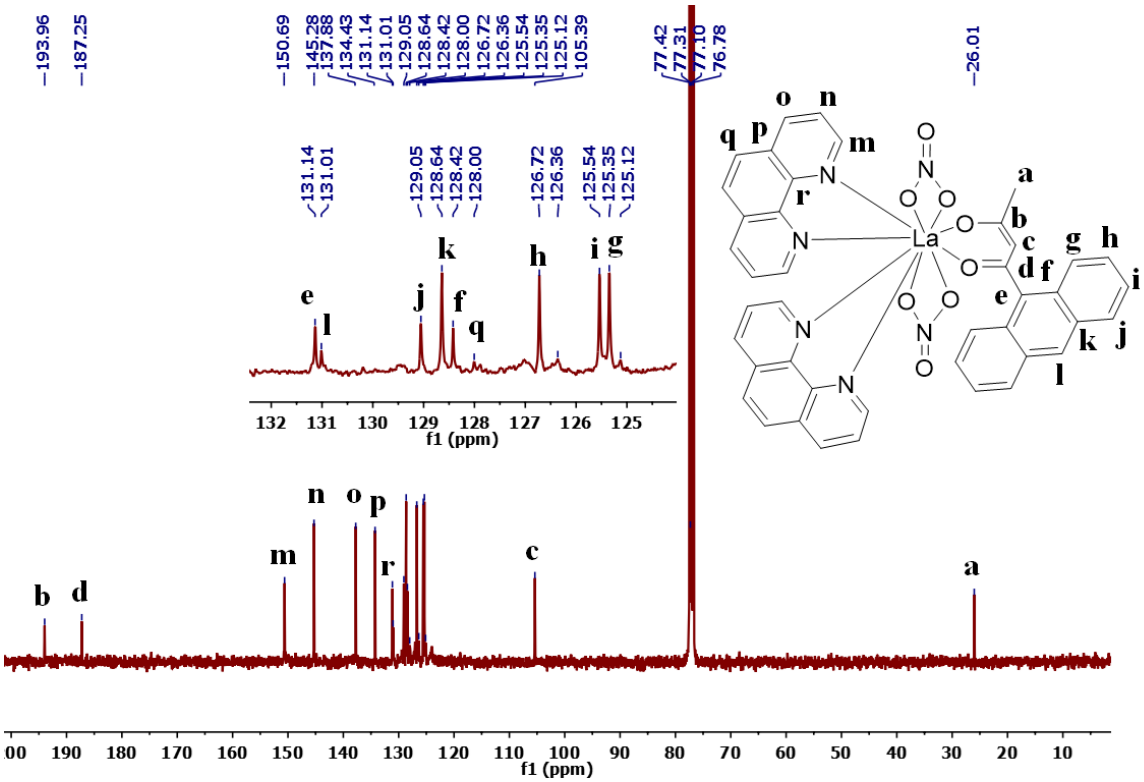

Figure S17: ^{13}C NMR of **2** recorded in $CDCl_3$ Bruker Avance 400 (100 MHz) spectrometer.

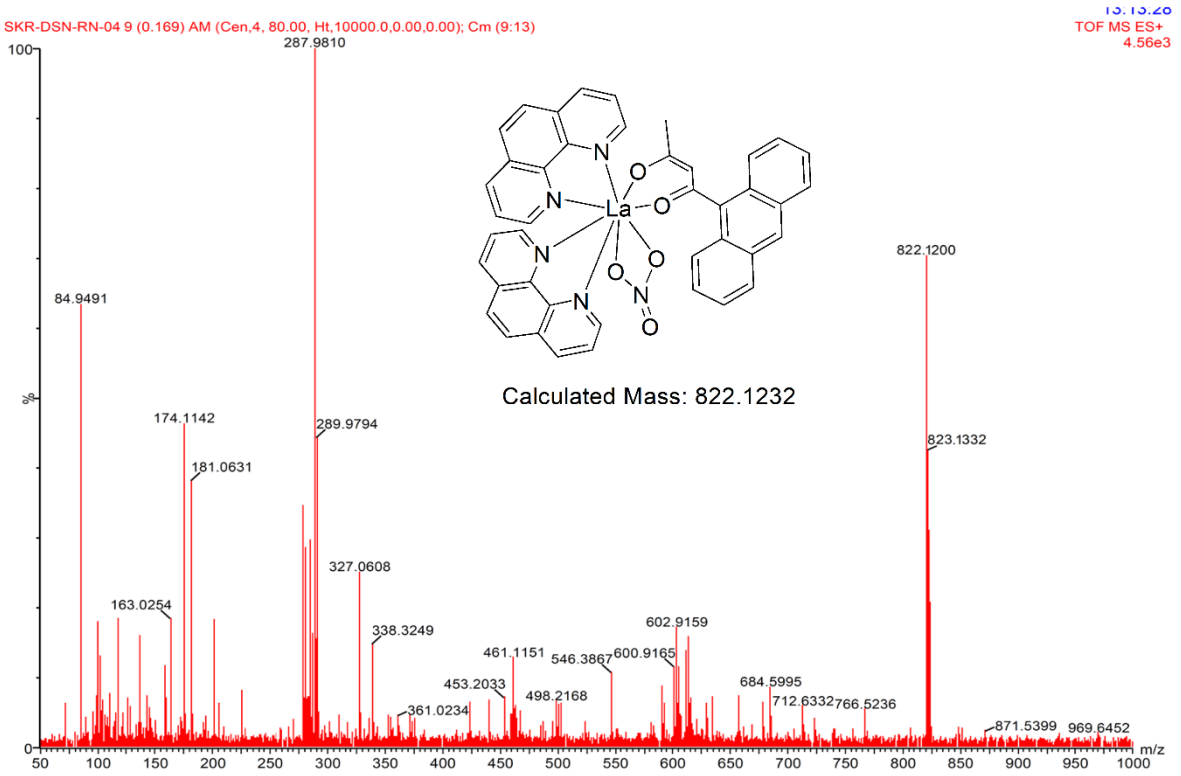

Figure S18: Q-TOF ESI Mass spectra of the **2** recorded in CH_3OH using Bruker Esquire 3000 Plus spectro-photometer (Bruker-Franzen Analytic GmbH, Bremen, Germany). The peak at m/z 822.1200 corresponds to the species $[M-(NO_3^-)]^+$.

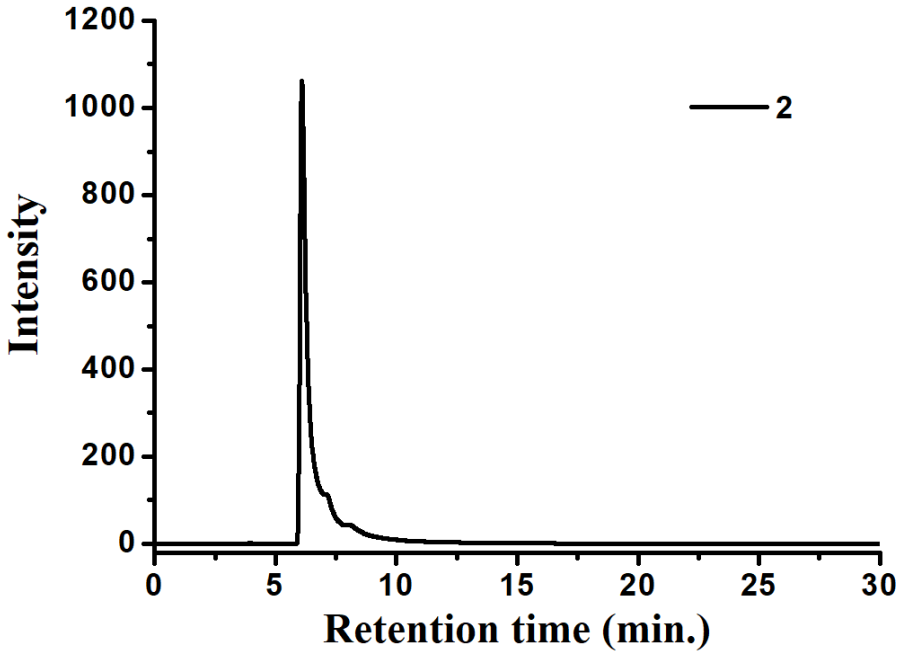

Figure S19: HPLC chromatograms for the complex (**2**) **(**Condition: UV = 254nm, flow rate 0.5 ml/min, solvent = H_2O: IPA = 95:5).

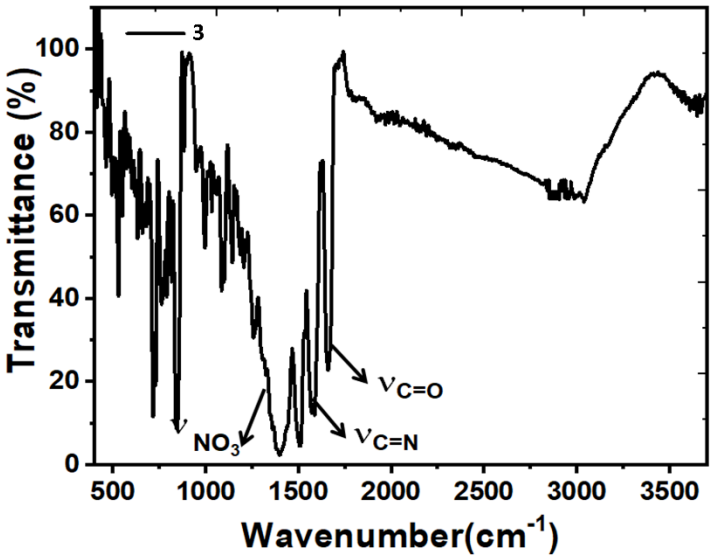

Figure S20: Solid phase FT-IR spectra of the complex **3**.

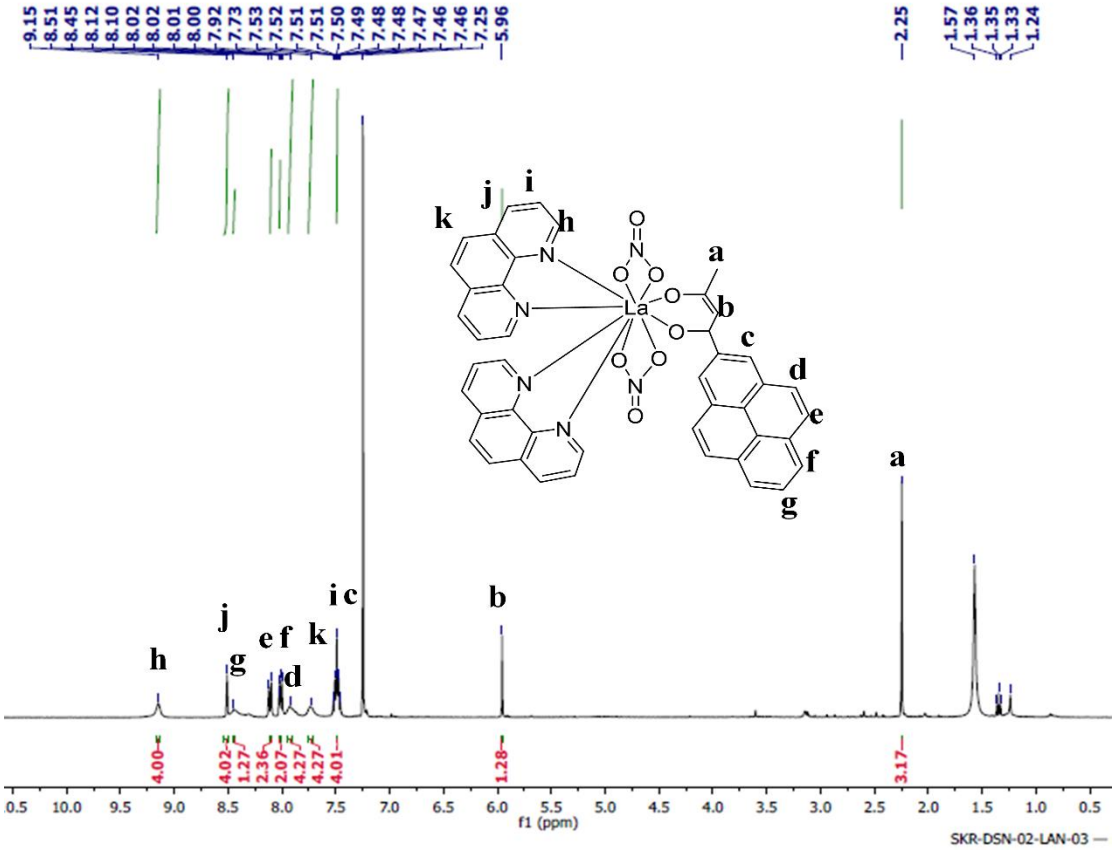

Figure S21: ^{1}H NMR of **3** recorded in $CDCl_3$ using Bruker Avance 400 (400 MHz) spectrometer.

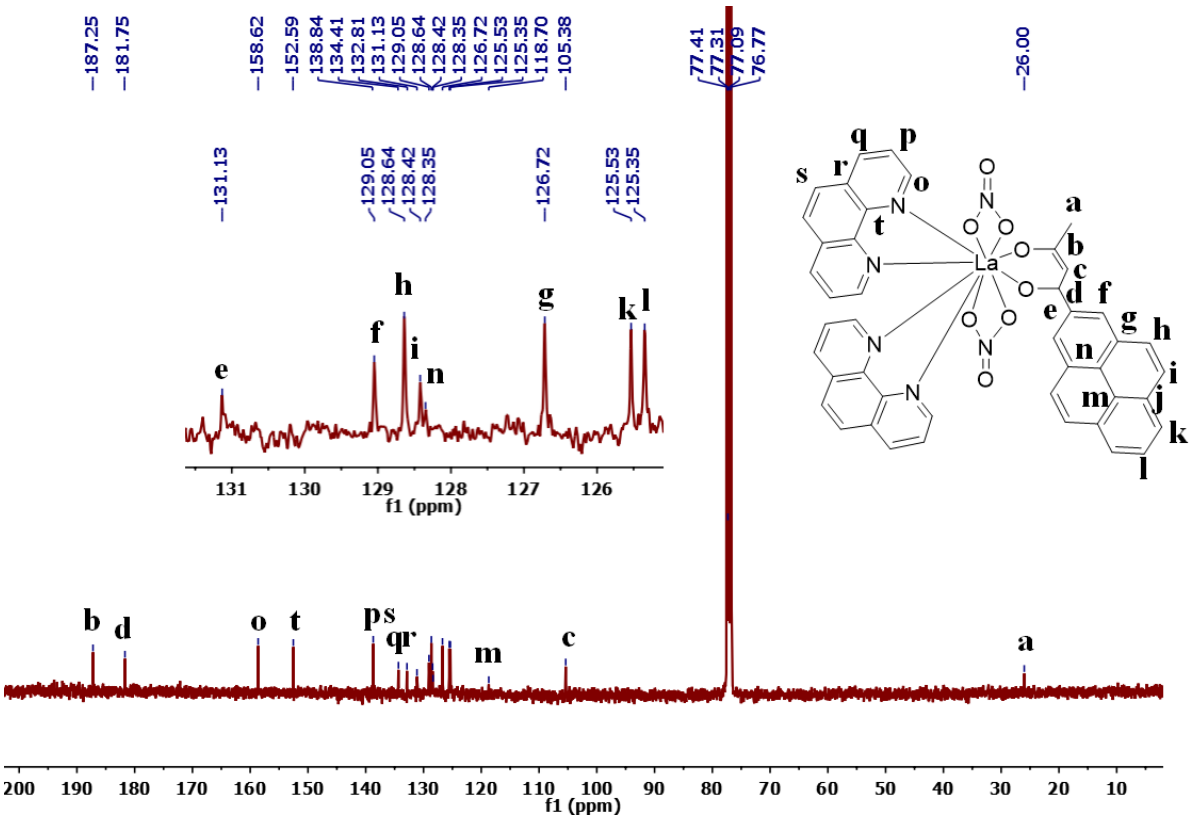

Figure S22: ^{13}C NMR of **1** recorded in $CDCl_3$ Bruker Avance 400 (100 MHz) spectrometer.

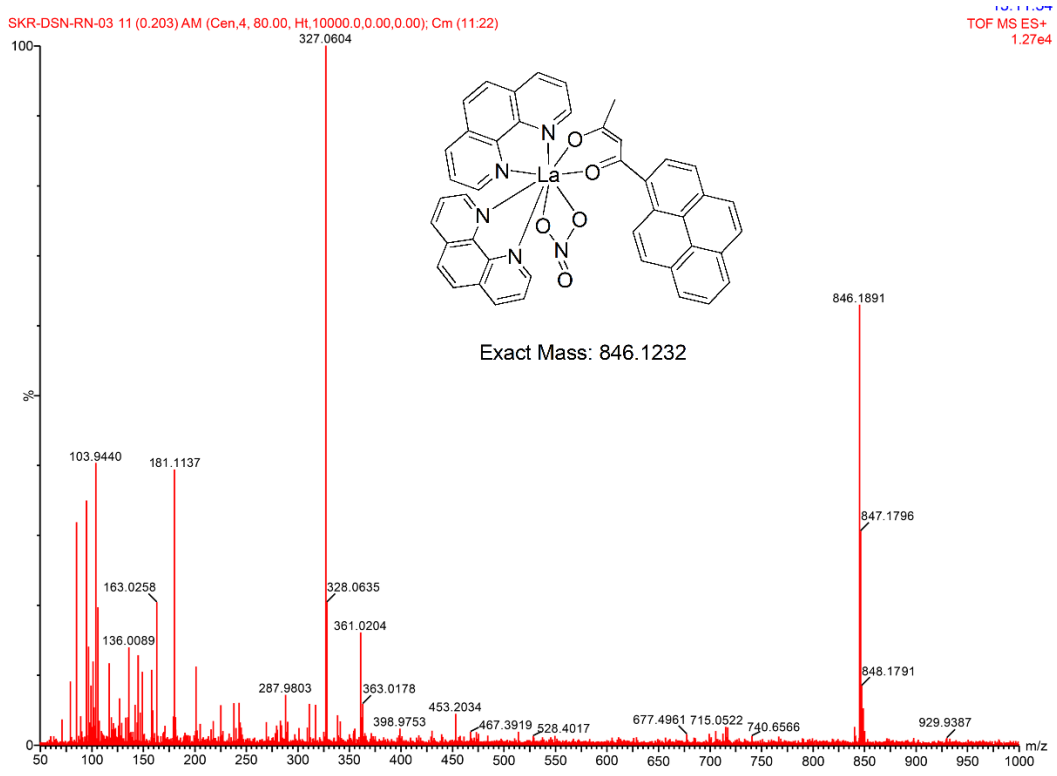

Figure S23: Q-TOF ESI Mass spectra of the **3** recorded in CH_3OH using Bruker Esquire 3000 Plus spectro-photometer (Bruker-Franzen Analytic GmbH, Bremen, Germany). The peak at m/z 846.1891 corresponds to the species $[M-(NO_3^-)]^+$.

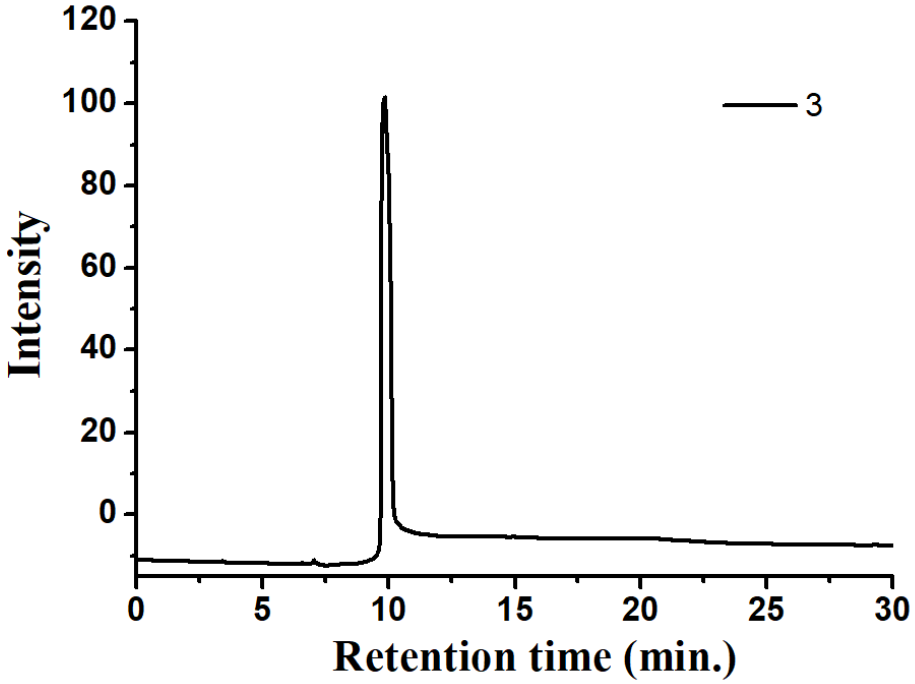

Figure S24: HPLC chromatograms for the complex (3) **(**Condition: UV = 254nm, flow rate 0.5 ml/min, solvent = H_2O: IPA = 95:5).

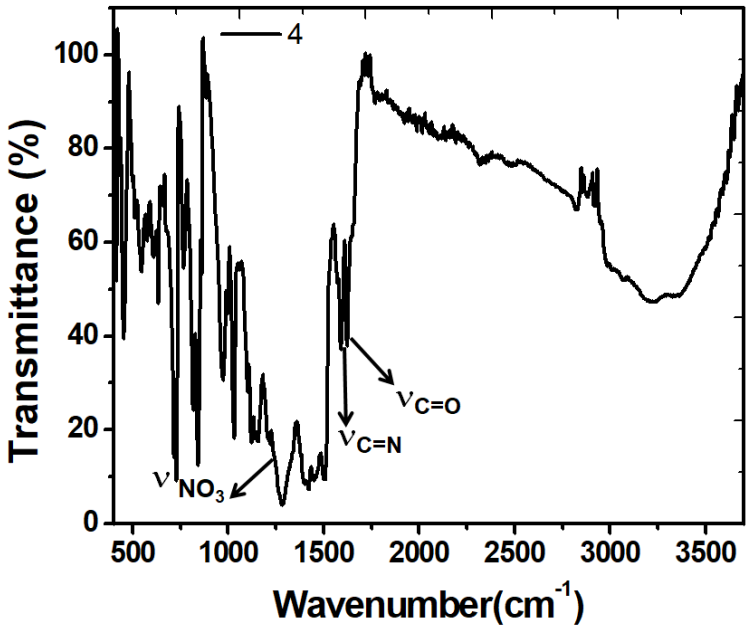

Figure S25: Solid phase FT-IR spectra of the complex 4.

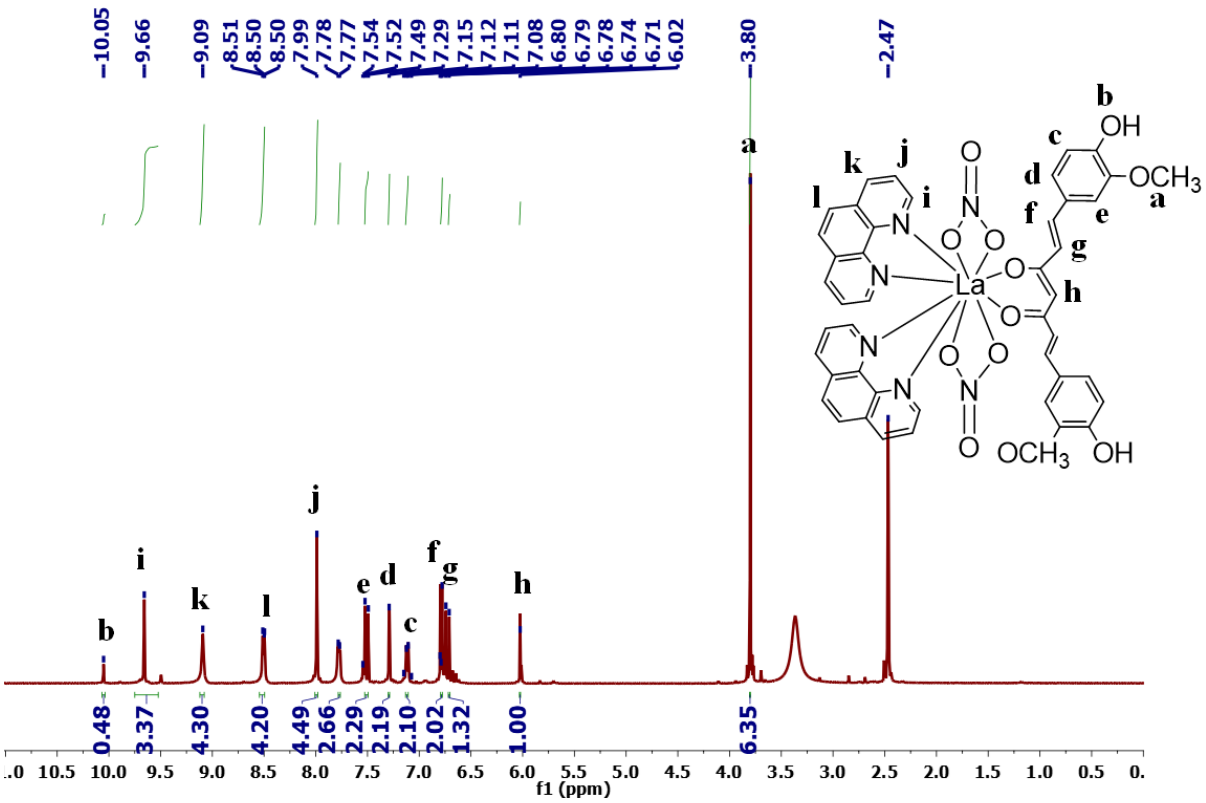

Figure S26: ^{1}H NMR of **4** recorded in DMSO-d$_6$ using Bruker Avance 400 (400 MHz) spectrometer.

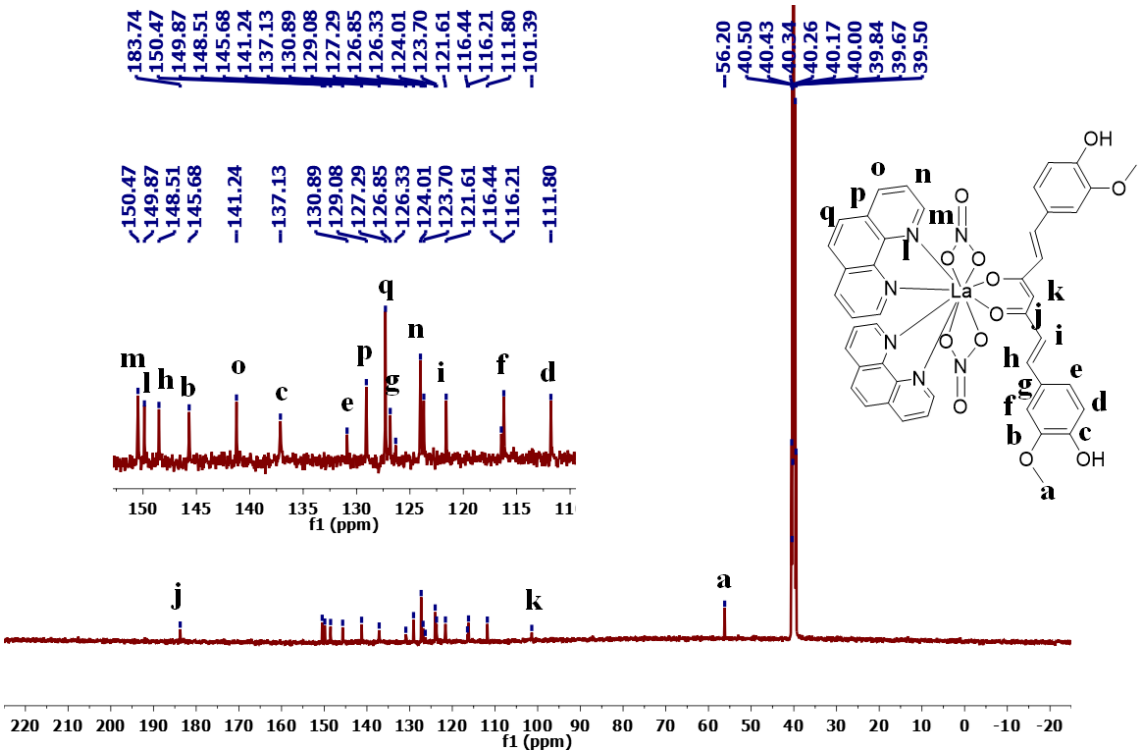

Figure S27: ^{13}C NMR of **4** recorded in DMSO-d$_6$ Bruker Avance 400 (100 MHz) spectrometer.

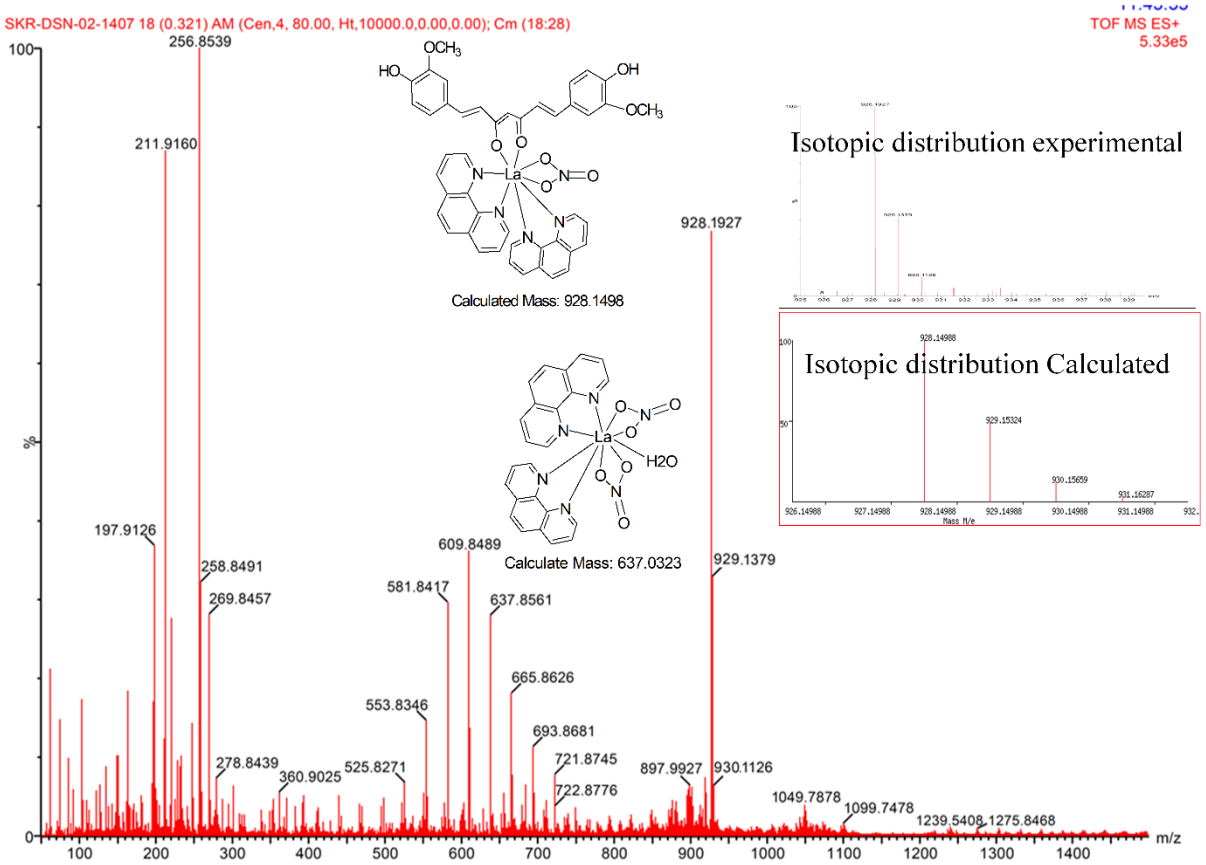

Figure S28: Q-TOF ESI Mass spectra of the **4** recorded in CH_3OH using Bruker Esquire 3000 Plus spectro-photometer (Bruker-Franzen Analytic GmbH, Bremen, Germany). The peak at m/z 928.1927 corresponds to the species $[M-(NO_3^-)]^+$.

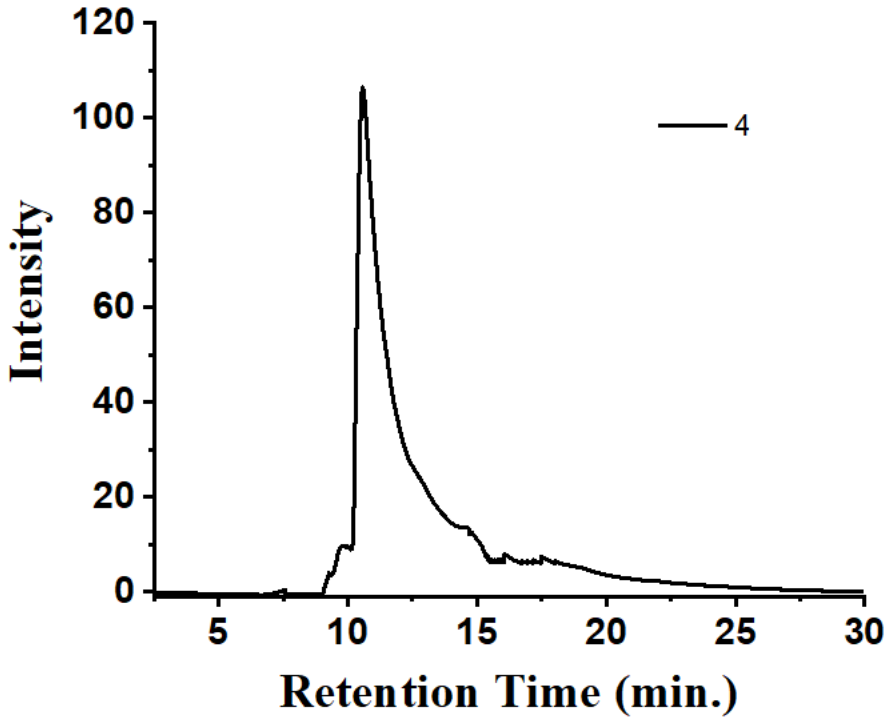

Figure S29: HPLC chromatograms for the complex (**4**) **(**Condition: UV = 254nm, flow rate 0.5 ml/min, solvent = H_2O: IPA = 95:5).

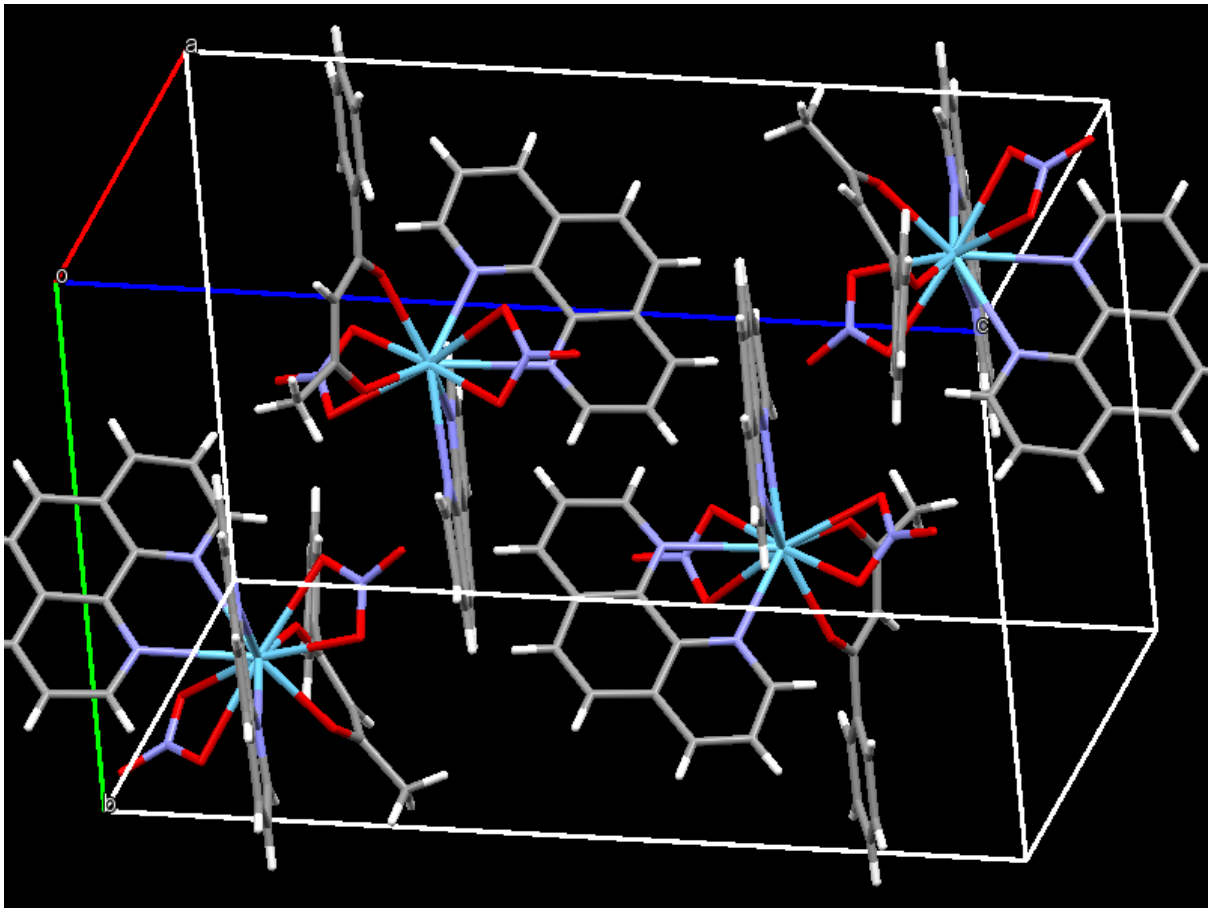

Figure S30: Unit cell packing diagram of **1**. Color code: N, blue; C, black; O, red; H, White.

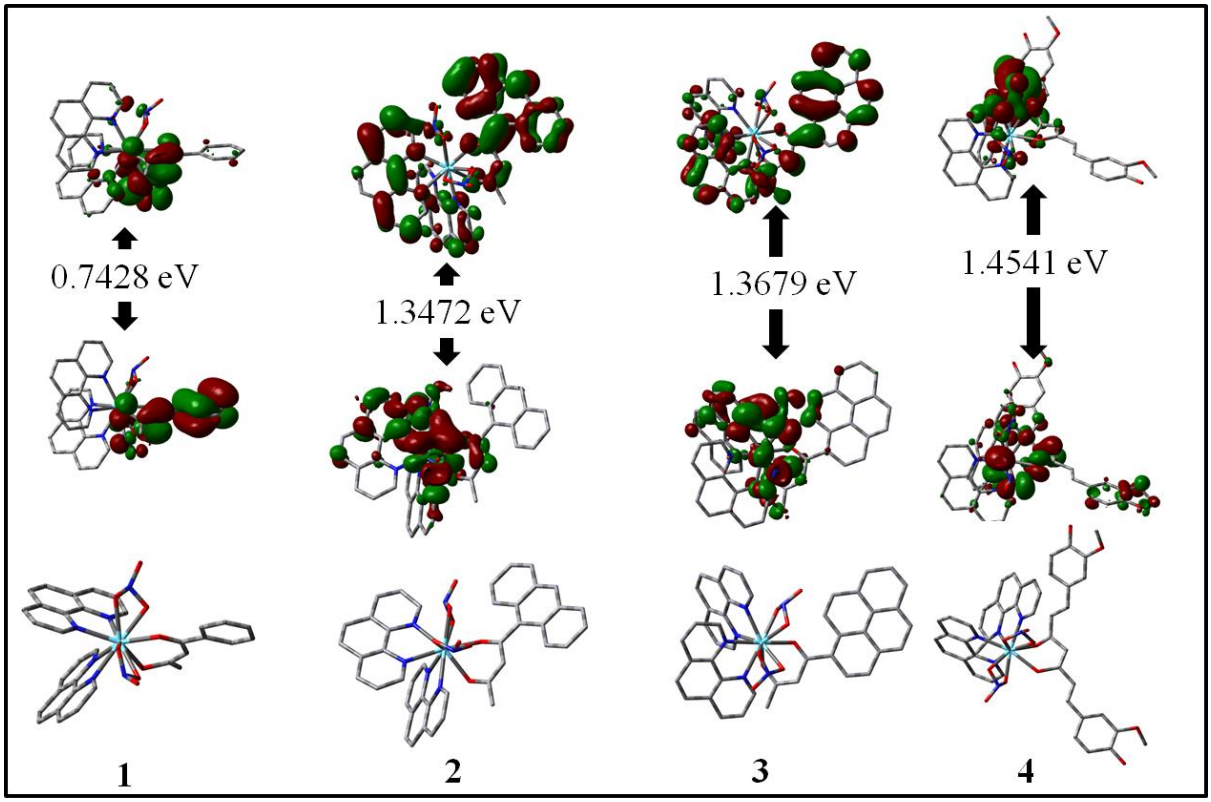

Figure S31: Optimized structure, HOMO and LUMO stereographs of the complexes from DFT calculation at DFT/CAM-B3LYP/6-31G(d)/LanL2DZ level using Gaussian 09W software.

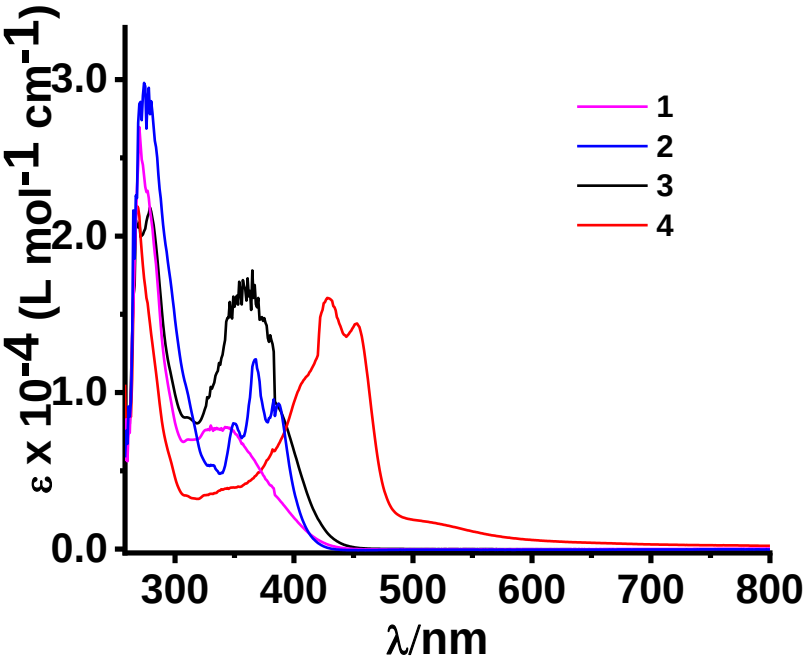

Figure S32: UV-Visible spectra of the complexes (**1-4**) in 5% DMSO-H_20.

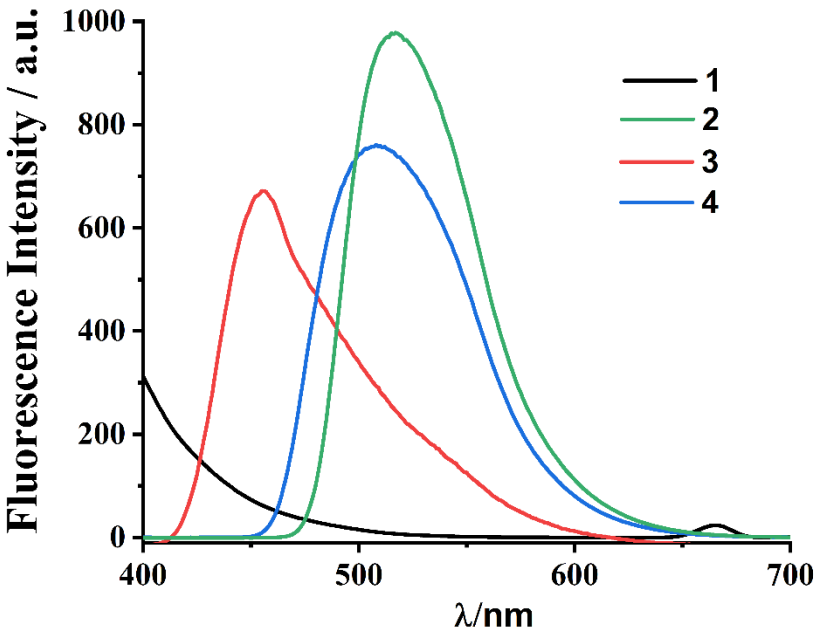

Figure 33: The emission spectra of the complexes (**1-4**) [100 µM] in 5% DMSO-H_20 (λ_{exc} = 375 nm (**1, 2, 3**); 430 nm (**4**)).

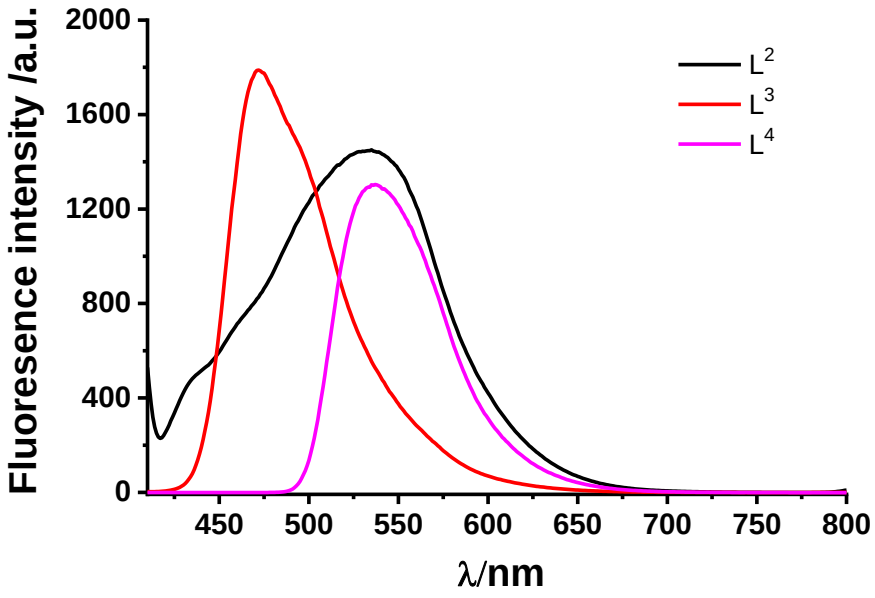

Figure S34: The emission spectra of the ligands (**L^2-L^4**) [100 µM] in 5% DMSO-H_20 (λ_{exc} = 375 nm (**L^2, L^3**); 430 nm (**L^4**)).

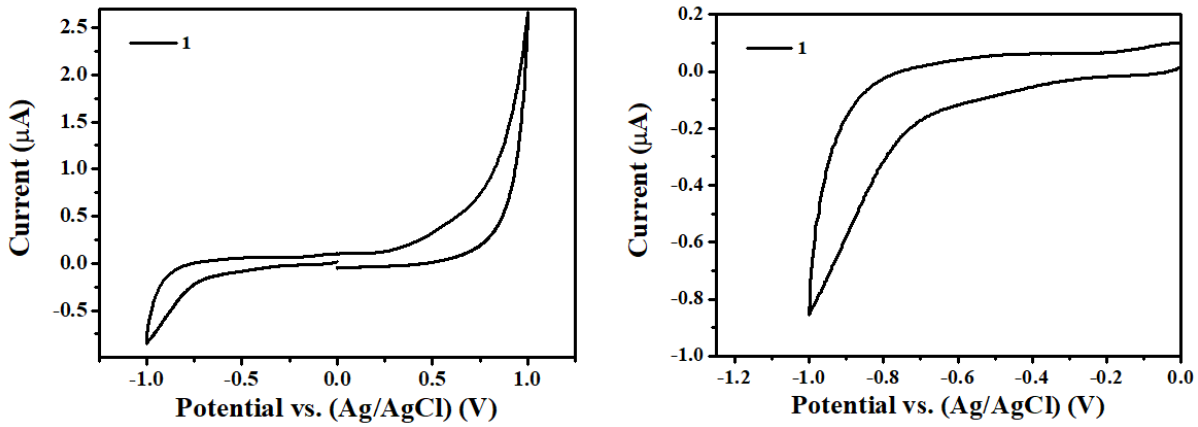

Figure S35: Cyclic Voltammogram of Complex **1 (**1 mM in DMF) is done using Glassy Carbon electrode as the working electrode, Ag/AgCl electrode as reference electrode and Pt electrode as counter electrode and TBAP (Tetrabutaylammonium perchlorate) 0.1 M as supporting electrolyte.

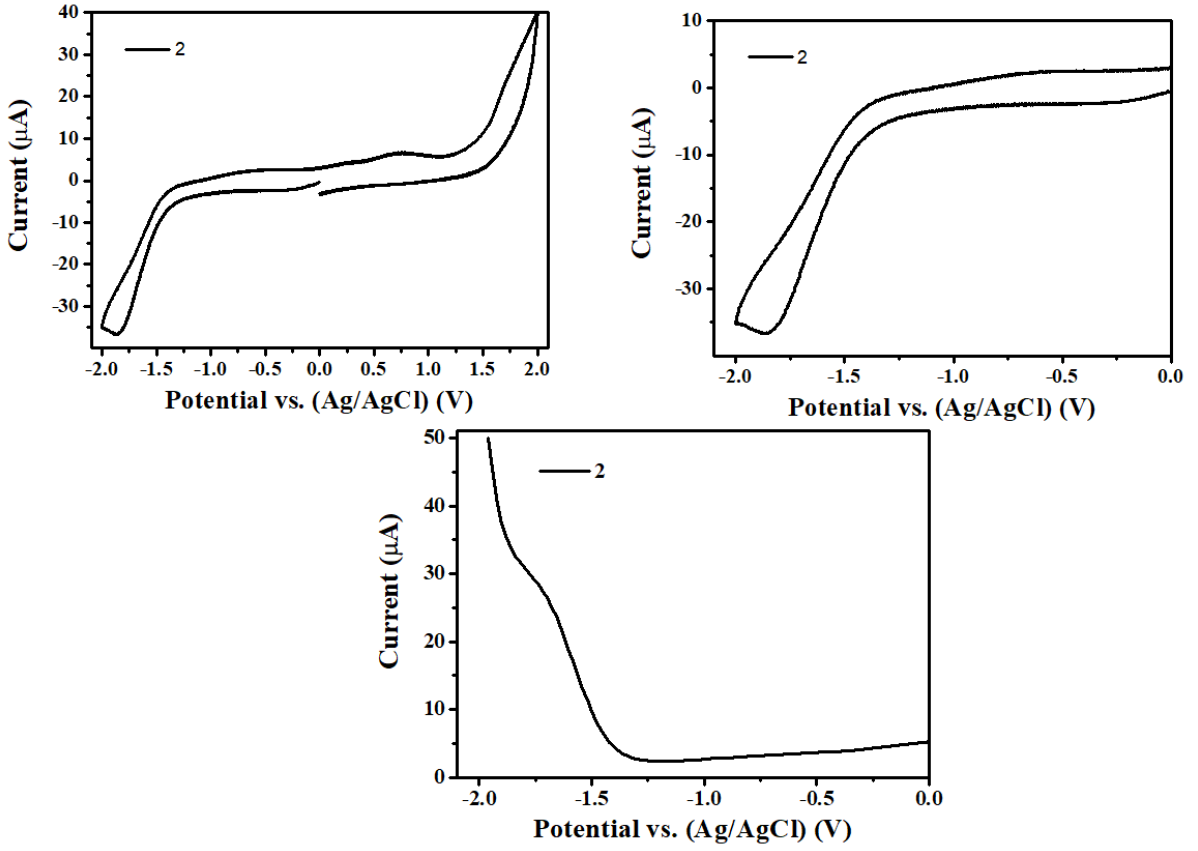

Figure S36: Cyclic Voltammogram and Differential Pulse Voltammetry of Complex **2 (**1mM in DMF) is done using Glassy Carbon electrode as the working electrode, Ag/AgCl electrode as reference electrode and Pt electrode as counter electrode and TBAP(Tetrabutaylammonium perchlorate) 0.1 M as supporting electrolyte.

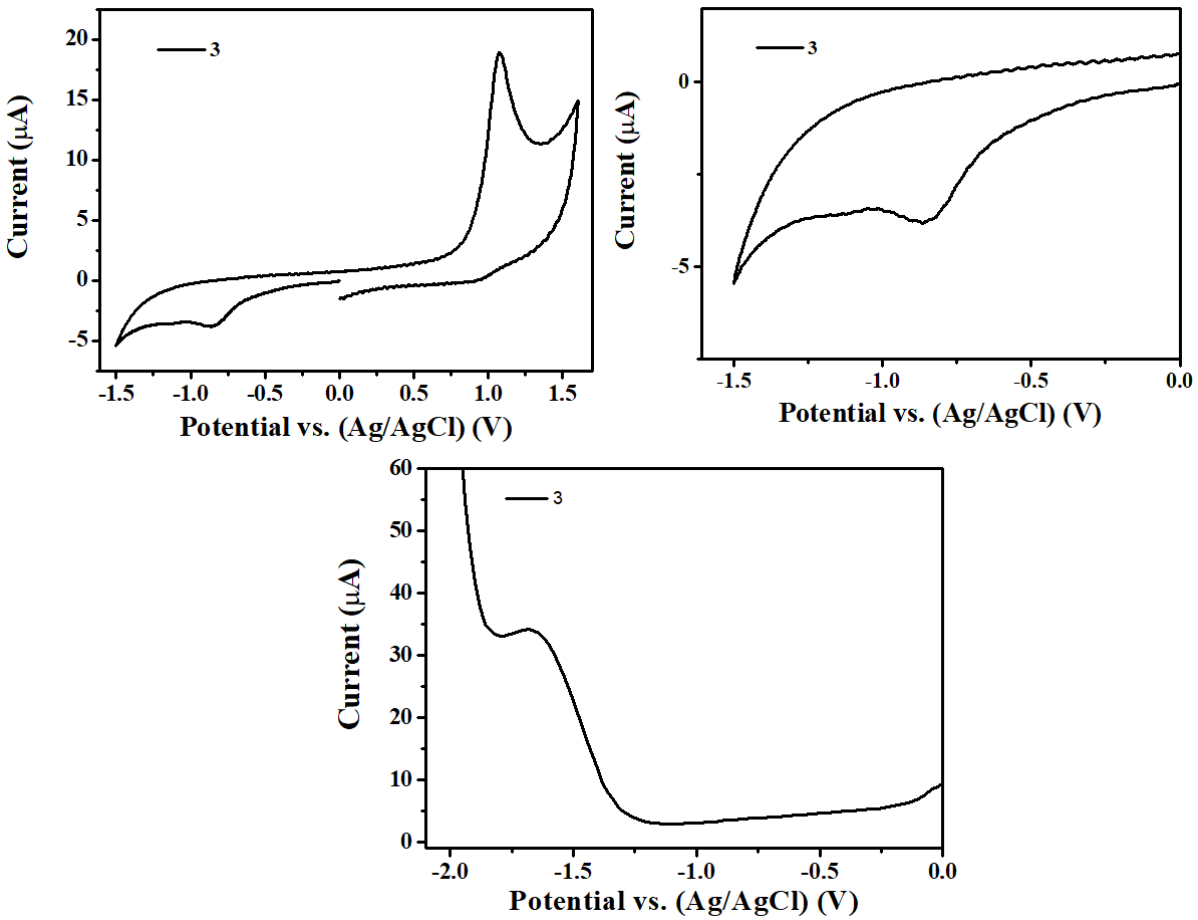

Figure S37: Cyclic Voltammogram and Differential Pulse Voltammetry of Complex **3 (**1mM in DMF) is done using Glassy Carbon electrode as the working electrode, Ag/AgCl electrode as reference electrode and Pt electrode as counter electrode and TBAP (Tetrabutaylammonium perchlorate) 0.1 M as supporting electrolyte.

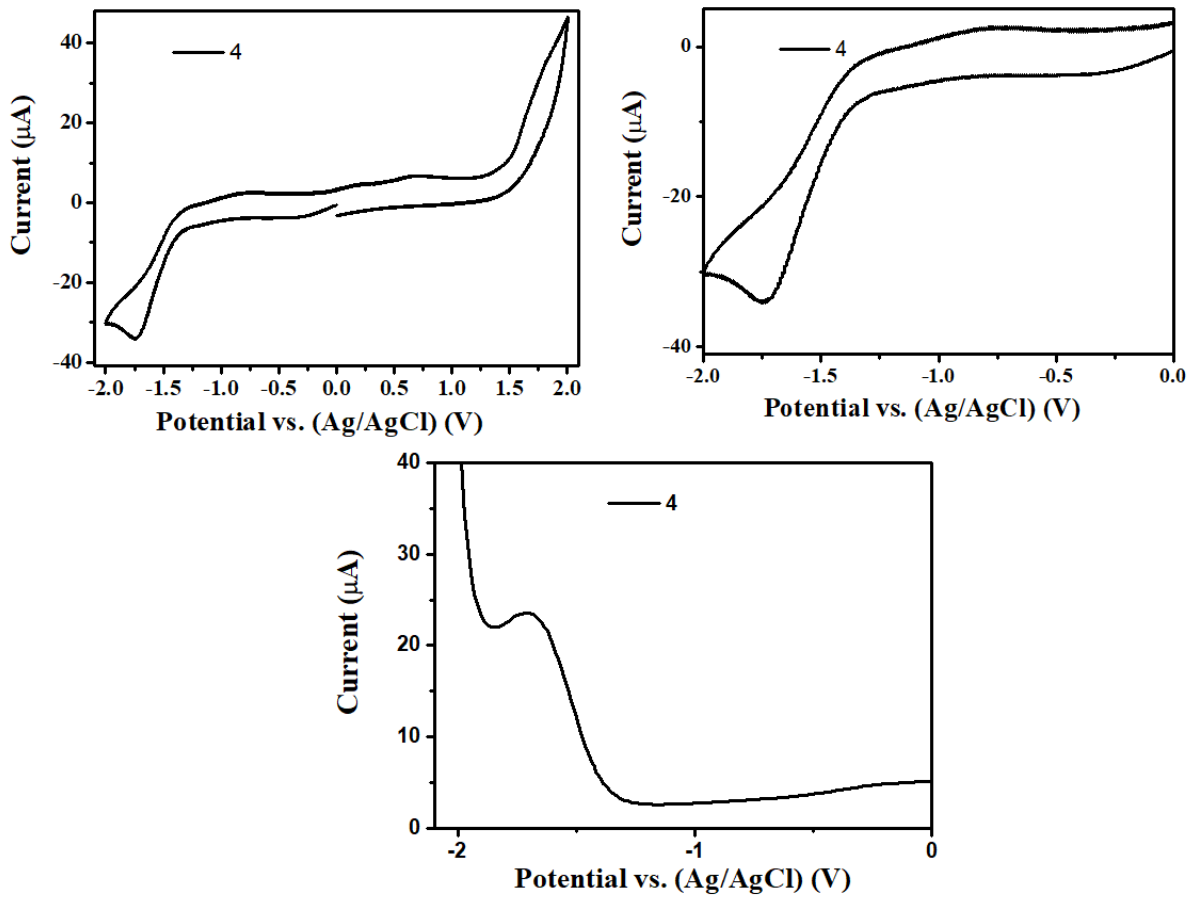

Figure S38: Cyclic Voltammogram and Differential Pulse Voltammetry of Complex **4 (**1mM in DMF) is done using Glassy Carbon electrode as the working electrode, Ag/AgCl electrode as reference electrode and Pt electrode as counter electrode and TBAP (Tetrabutaylammonium perchlorate) 0.1 M as supporting electrolyte.

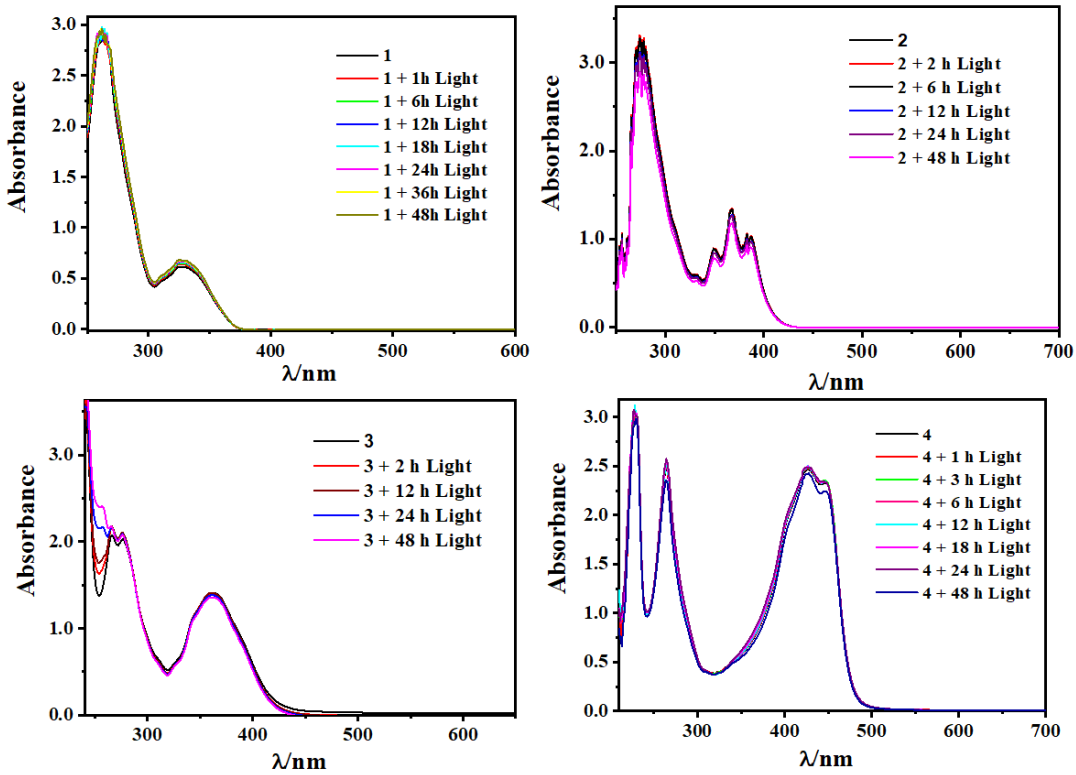

Figure S39: UV-Visible spectral measurements of complexes 1-4 in 5% v/v DMSO-H_2O in presence of light (400-700 nm, 10 J cm^{-2}), where spectral traces were recorded at different time intervals till 48h.

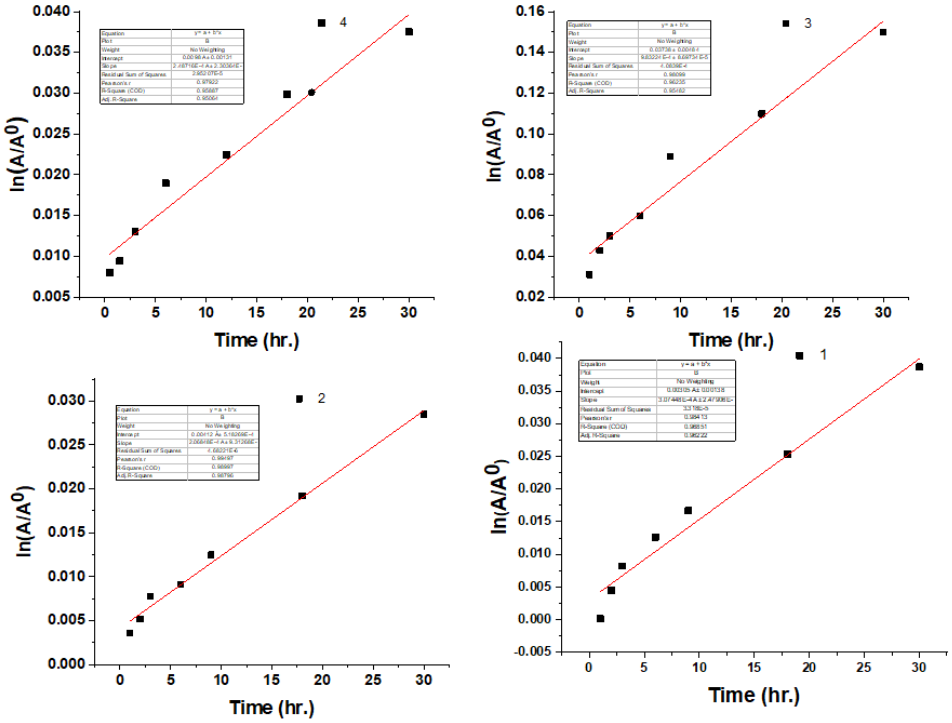

Figure S40: Determination of rate of dissociation (h^{-1}) of the complexes (**1-4**) in 1% DMSO/Dulbecco's modified Eagle's medium (DMEM) in presence of light (400-700 nm, 10 J cm^{-2}), where spectral traces were recorded at different time intervals till 30h.

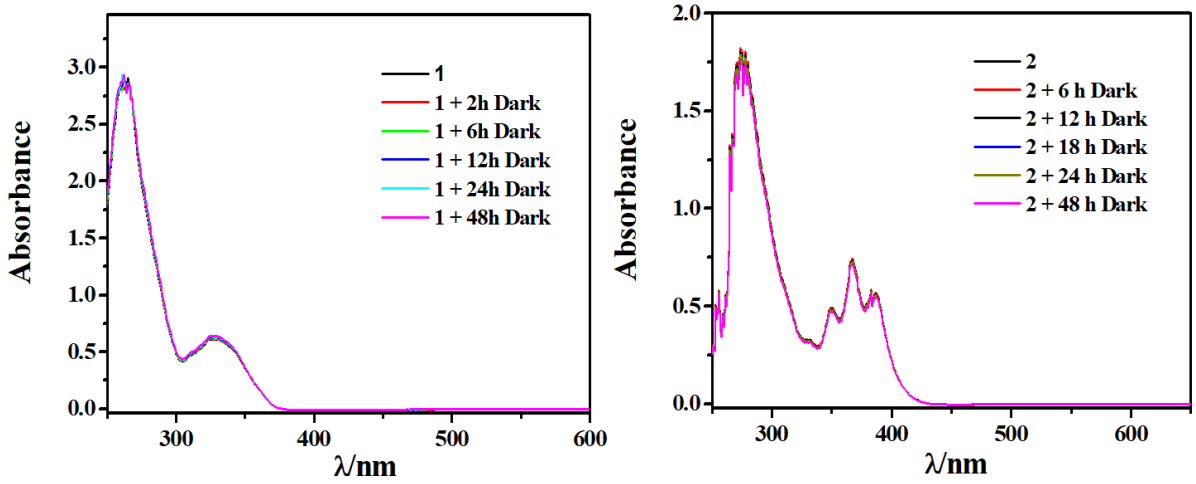

Figure S41: UV-Visible spectral measurements of complexes 1 and 2 in 5% v/v DMSO-H_2O in dark, where spectral traces were recorded at different time intervals till 48h.

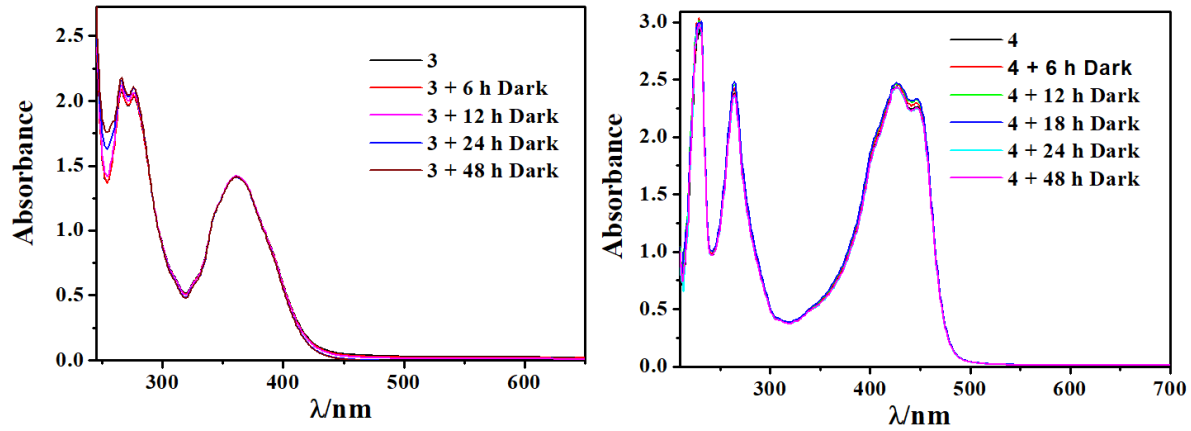

Figure S42: UV-Visible spectral measurements of complexes 3 and 4 in 5% v/v DMSO-H_2O in dark, where spectral traces were recorded at different time intervals till 48h.

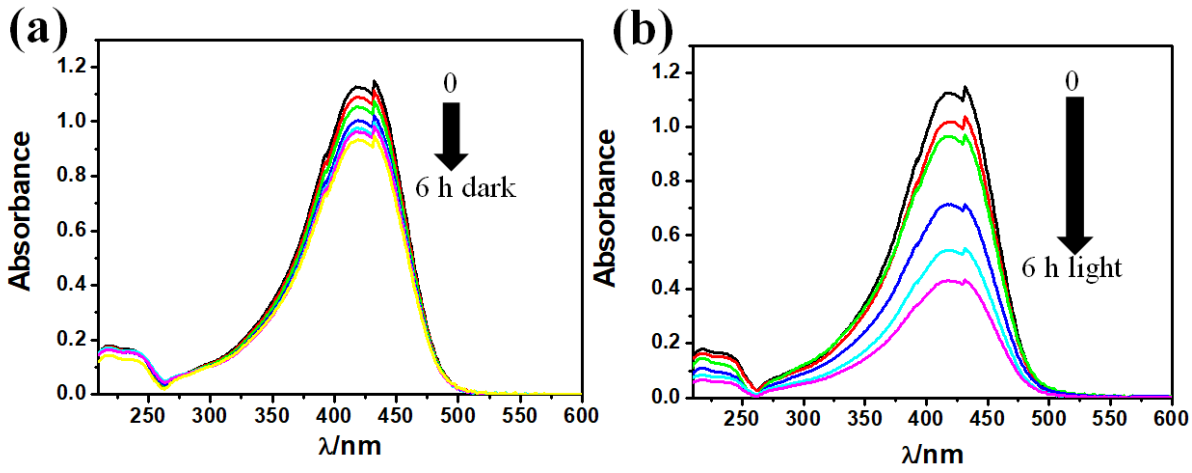

Figure S43: UV-Visible spectral measurements of the ligand (L^4) in (a) dark and (b) presence of light (400-700 nm, 10 J cm^{-2}) in 5% v/v DMSO-H_2O, where spectral traces were recorded at different time intervals till 6 h.

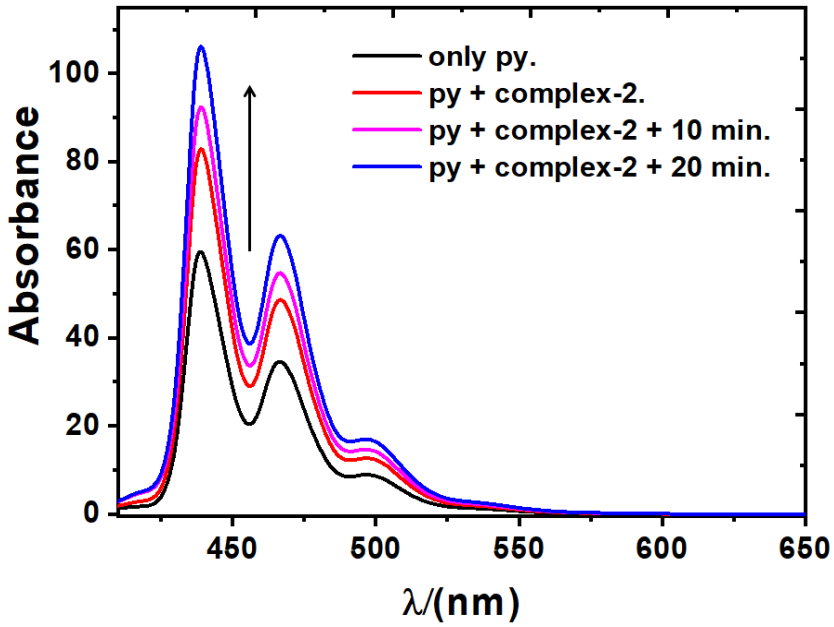

Figure S44: Up-conversion emission spectra of the complex (2) and acceptor (Perylene) after 20 min. light (400-700 nm, 10 J cm^{-2}) recorded in CH_3CN indicating the presence of triplet excited state in the complex; [complex] = 50 µM, [Perylene] = 250 µM (λ_{ex} = 375 nm).

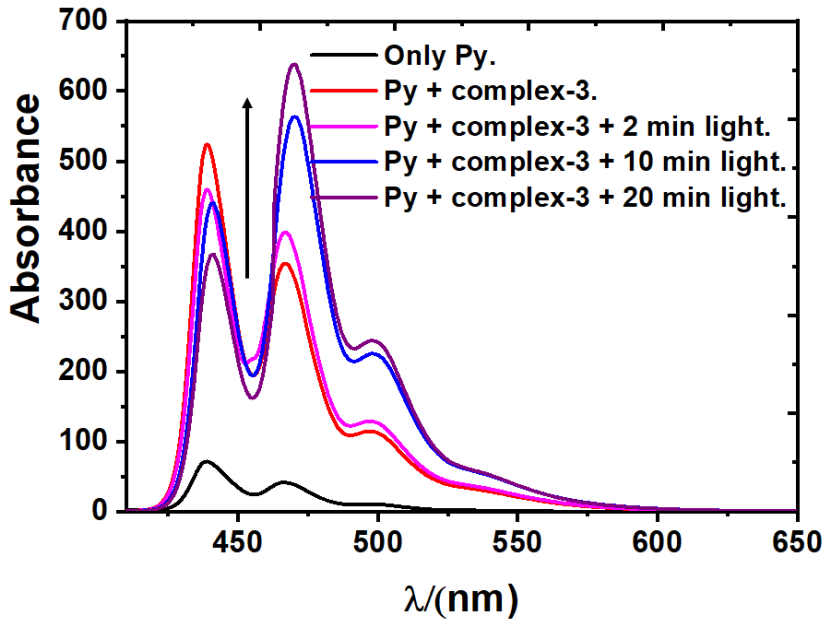

Figure S45: Up-conversion emission spectra of the complex (3) and acceptor (Perylene) after 20 min. light (400-700 nm, 10 J cm^{-2}) recorded in CH_3CN indicating the presence of triplet excited state in the complex; [complex] = 50 µM, [Perylene] = 250 µM (λ_{ex} = 375 nm).

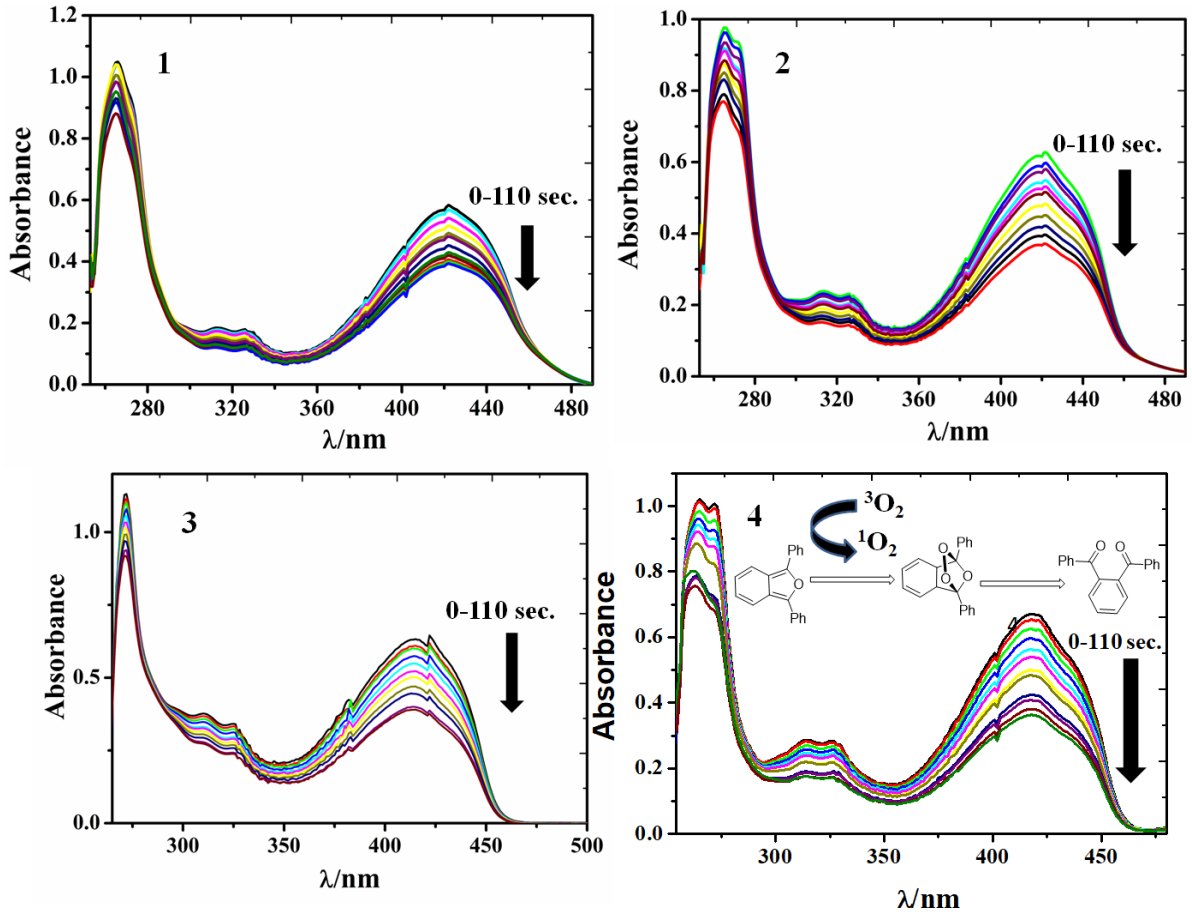

Figure S46: UV-Visible absorbption spectral traces of diphenylisobenzofuran (DPBF) (50µM) treated with the complexes (1-4) (20µM) on exposure to visible light (400-700 nm,10 J cm^{-2}) in an interval upto 110 sec.

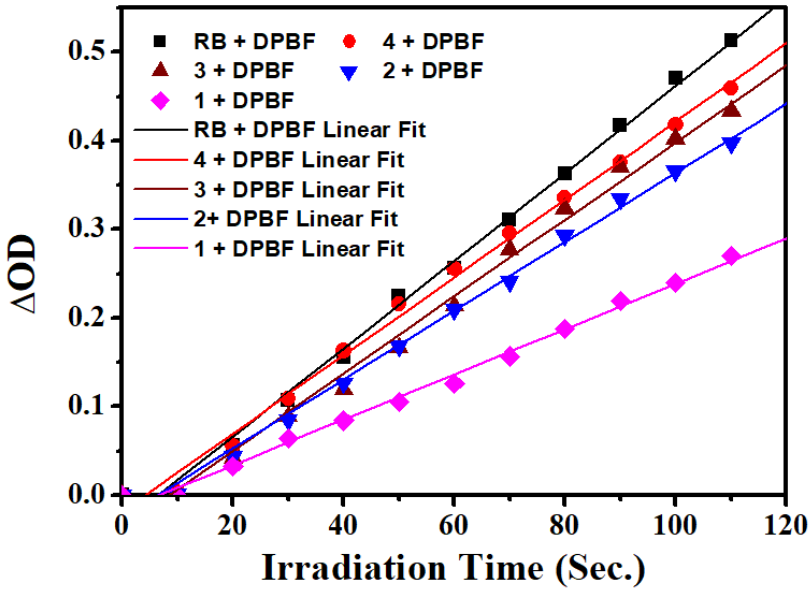

Figure S47: Plot of the relative change of the absorbance of DPBF at 417 nm with time of visible light (400-700 nm, 10 J cm^{-2}) exposure treated with the complexes (**1**-**4**) and Rose Bengal (reference) showing a linear decrease of the DPBF absorbance indicating photo-induced generation of singlet oxygen in type II photo-process.

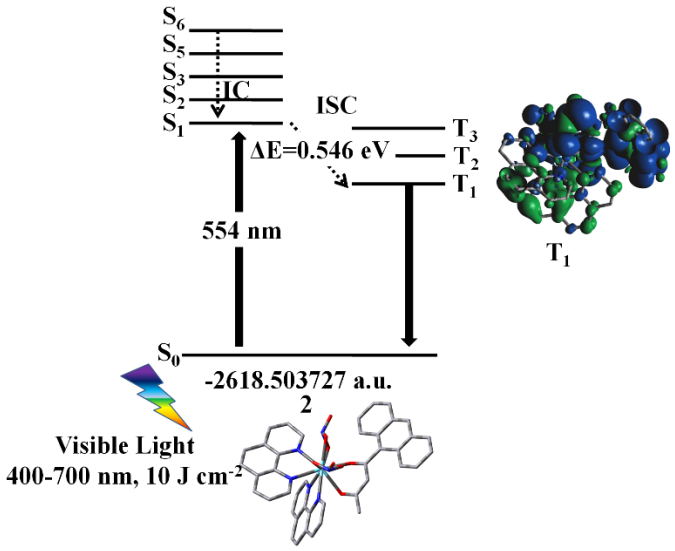

Figure 48. Proposed type-II photo-process and energetics in the complex 2 on photo-activation. Calculated at TD-DFT/CAM-B3LYP/6-31G(d,p)/LanL2DZ level in gas phase with Gaussian 09W.

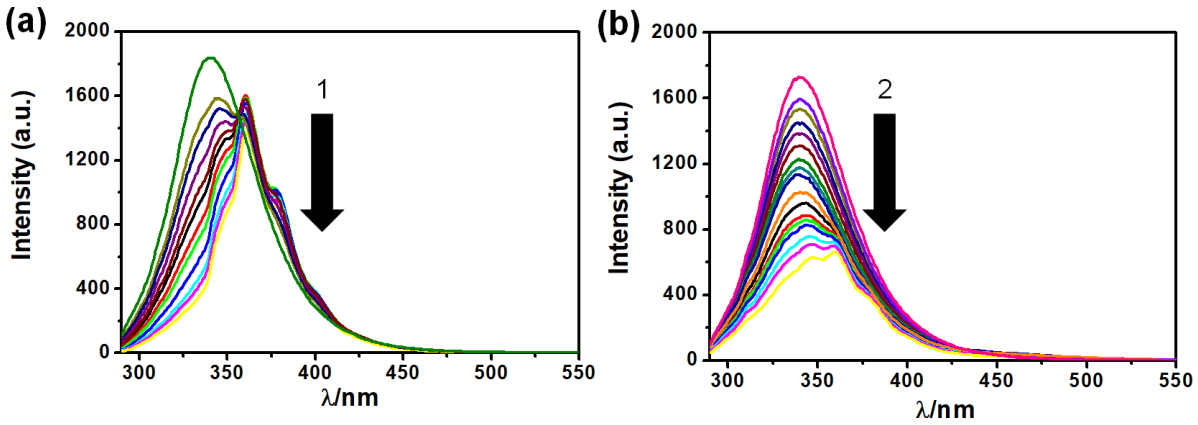

Figure S49: Fluorescence spectral traces of BSA showing the quenching effect in addition of (a) complex 1 and (b) 2 in Tris-HCl buffer (5 mM, pH 7.2) at 25^0c.

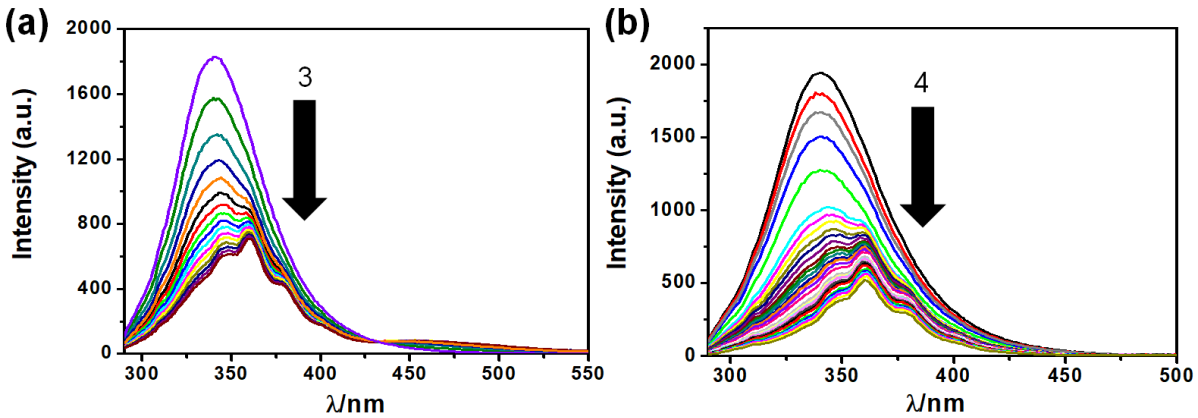

Figure S50: Fluorescence spectral traces of BSA showing the quenching effect in addition of (a) complex 3 and (b) 4 in Tris-HCl-buffer (5 mM, pH 7.2) at 25^0c.

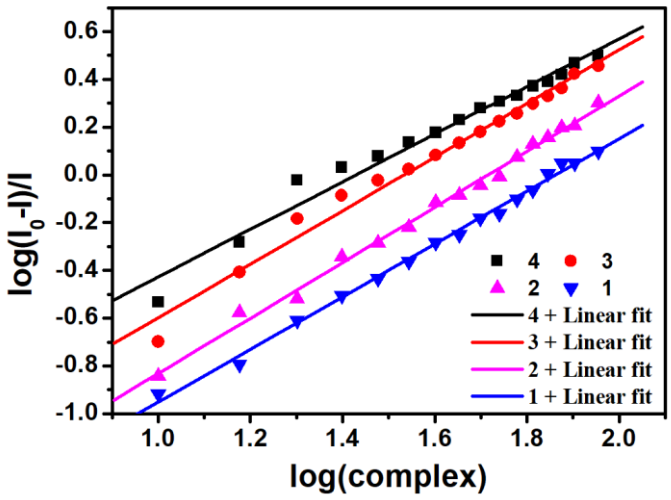

Figure S51: Scatchard plots between log (I_0-I)/I (λ_{ex}=295 nm), [BSA]=20 µM vs. log[complex] of all complexes (1-4).

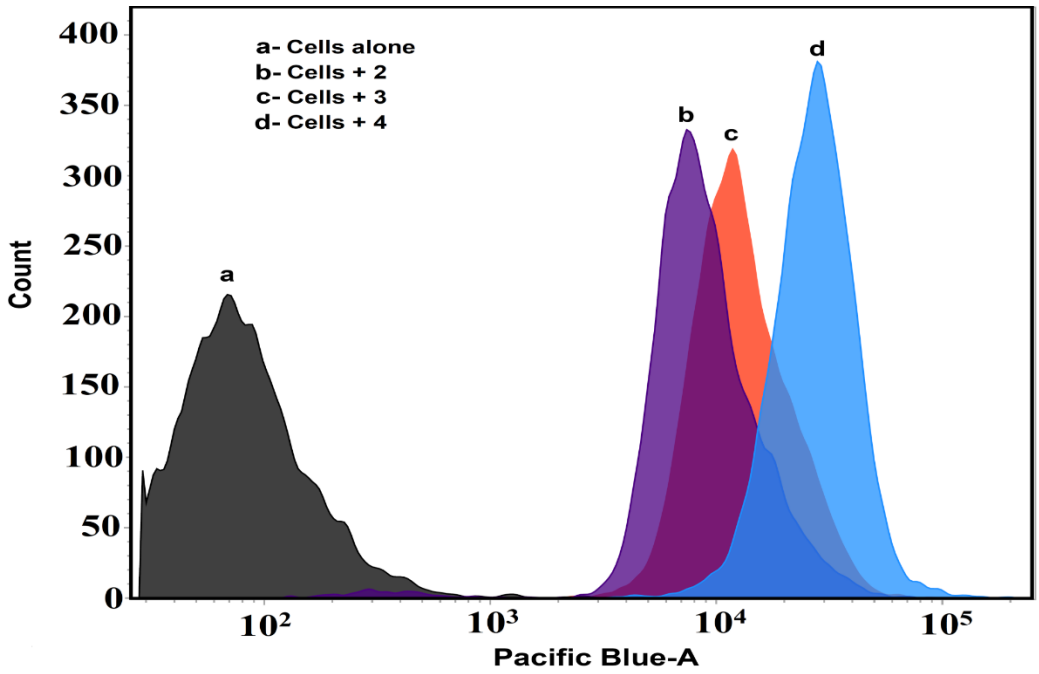

Figure 52: The FACS data from the cellular uptake study of complexes 2, 3 and 4 (5µM) in HeLa cells after 4 h incubation.

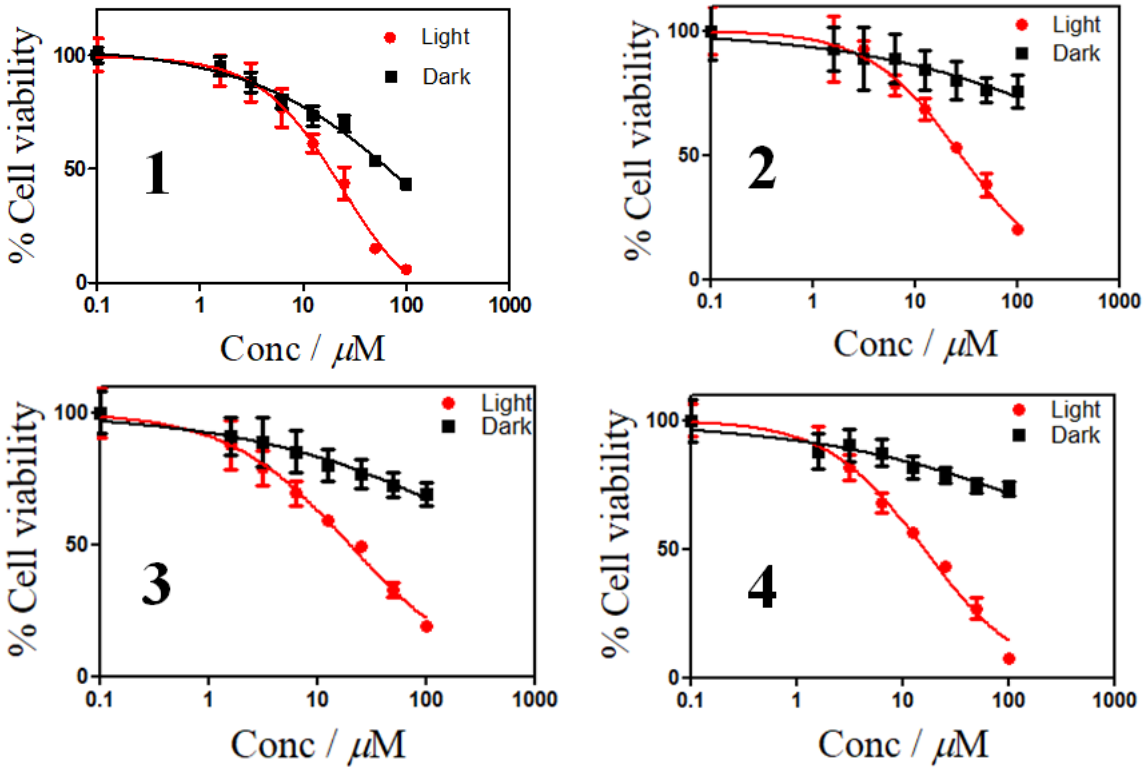

Figure S53: Cell viability (MTT assay) plots showing the cytotoxicity of the Lanthanium (III) complexes (**1 - 4**) in HeLa cells in the dark (black symbols) and in the presence of visible light (red symbols, 400-700 nm, 10 J cm^{-2}). The number inside the plot indicates the complex.

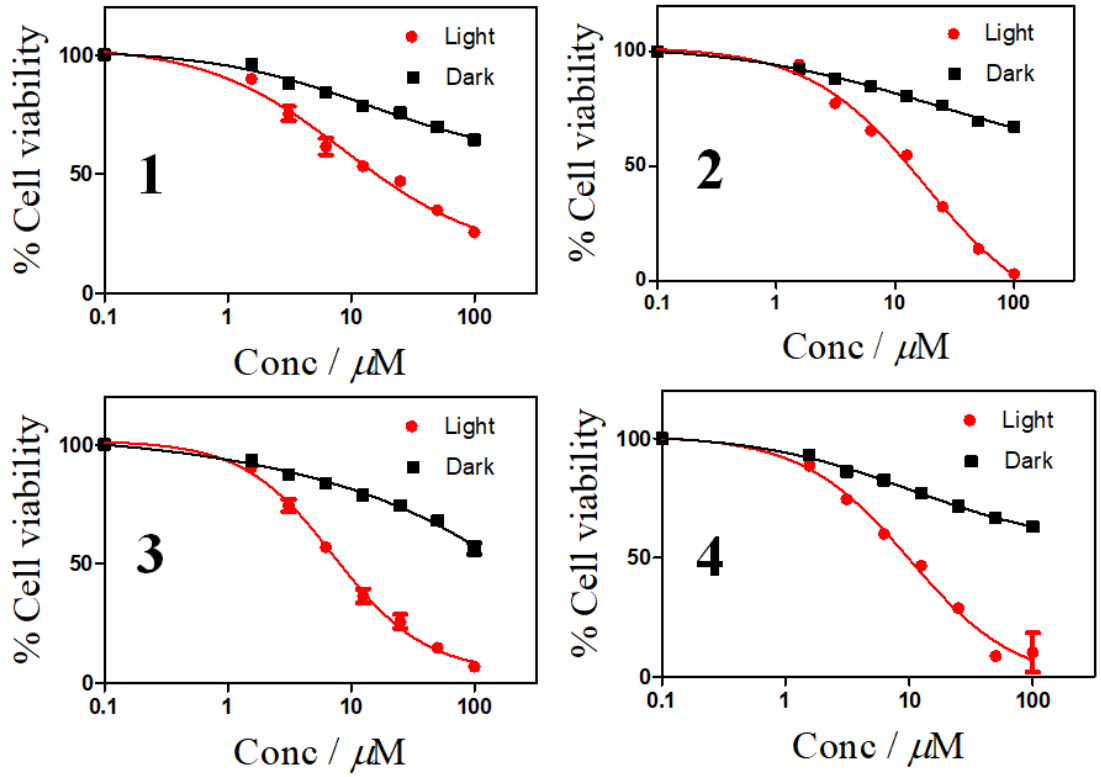

Figure S54: Cell viability (MTT assay) plots showing the cytotoxicity of the Lanthanium (III) complexes (**1 - 4**) in MCF-7 cells in the dark (black symbols) and in the presence of visible light (red symbols, 400-700 nm, 10 J cm^{-2}). The number inside the plot indicates the complex.

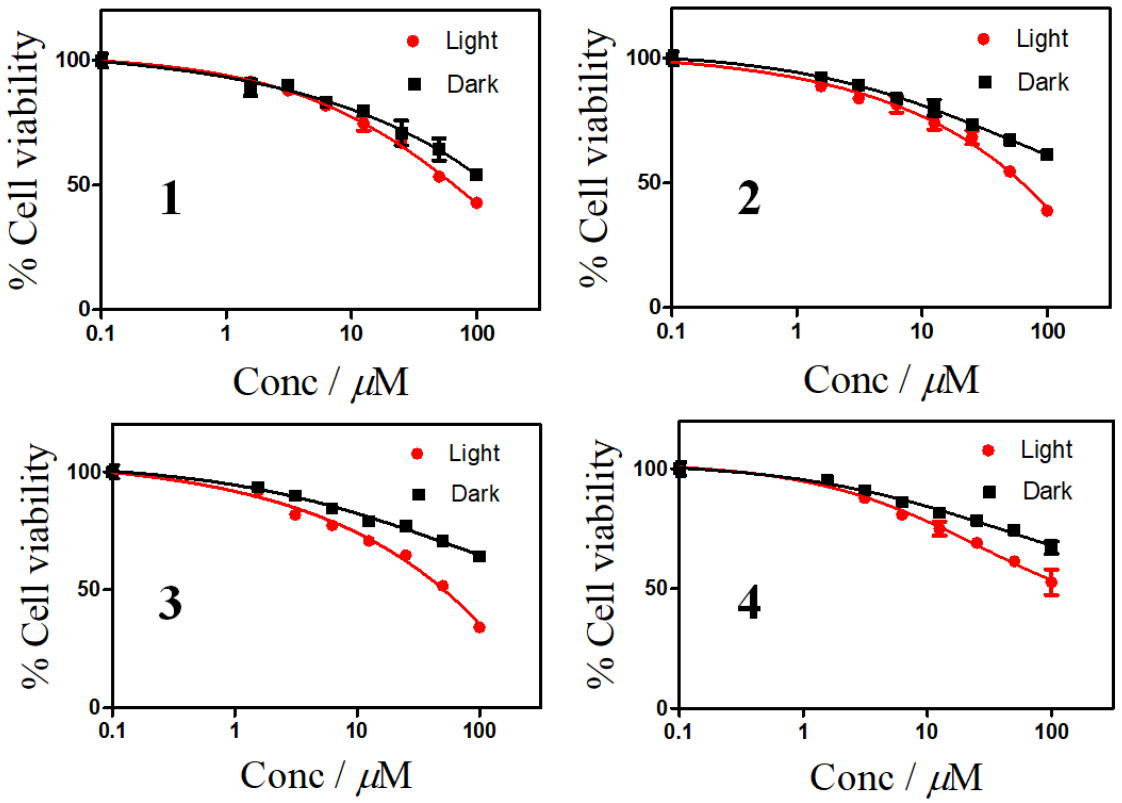

Figure S55: Cell viability (MTT assay) plots showing the cytotoxicity of the Lanthanium (III) complexes (**1 - 4**) in MCF-10 cells in the dark (black symbols) and in the presence of visible light (red symbols, 400-700 nm, 10 Jcm^{-2}). The number inside the plot indicates the complex.

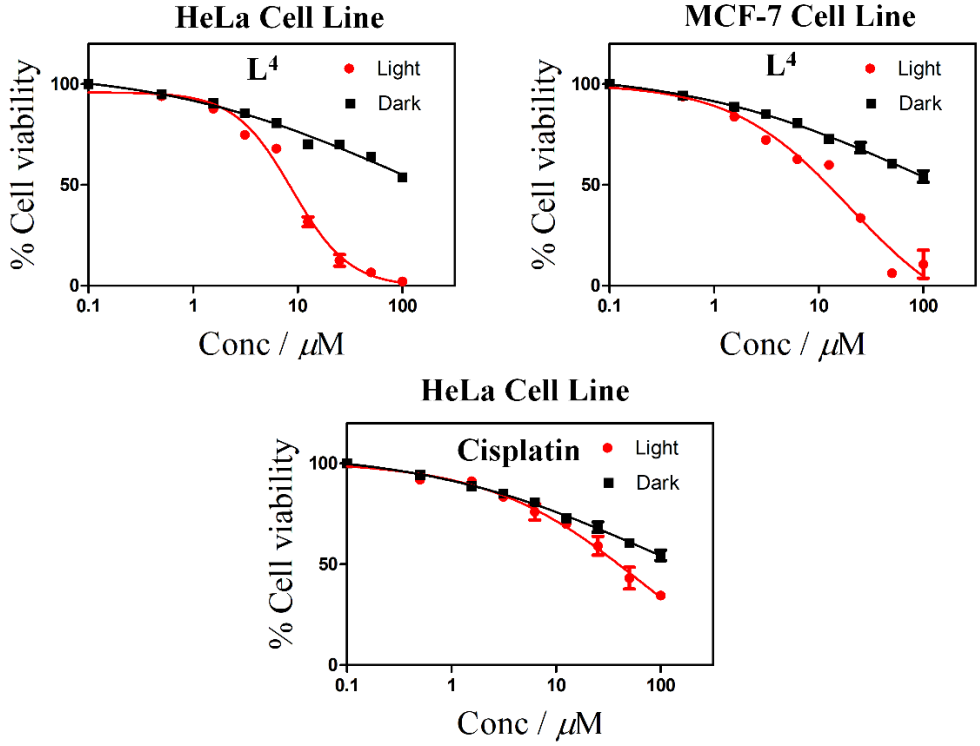

Figure S56: Cell viability (MTT assay) plots showing the cytotoxicity of the Curcumin (L^4) and Cisplatin in HeLa and MCF-7 cells in the dark (black symbols) and in the presence of visible light (red symbols, 400-700 nm, 10 Jcm^{-2}).

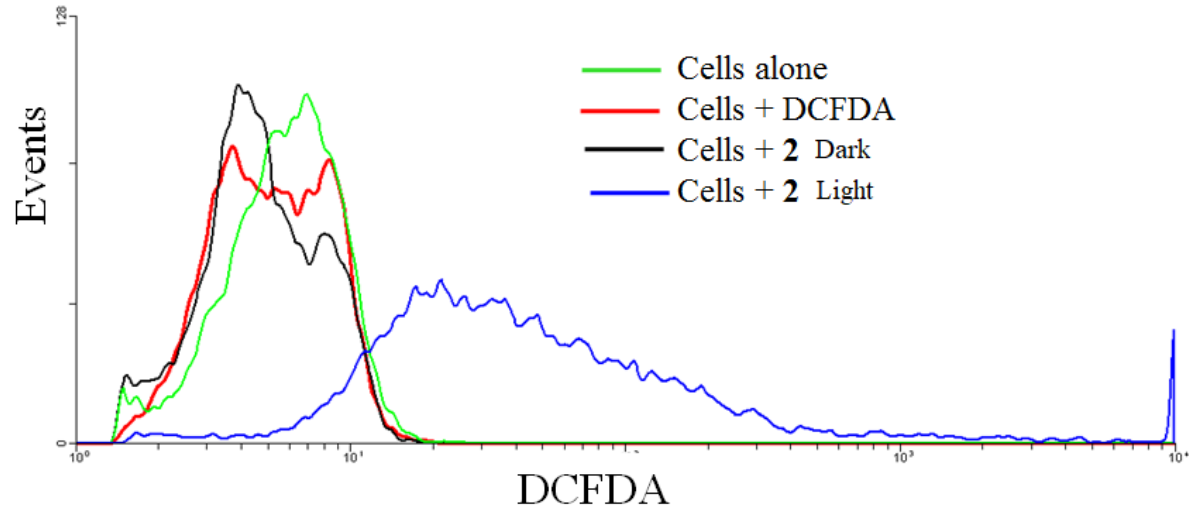

Figure S57: Fluorescence Assisted Cell Sorting (FACS) analysis for in vitro ROS generation in HeLa cells by photo-activated complex 2 (5 μM) using DCFDA dye. Generation of ROS was marked by the shift in fluorescence band positions compared to cells alone in HeLa cells treated with complexes in dark or visible light (400-700 nm, 10 J cm-2), as shown by the different color codes.

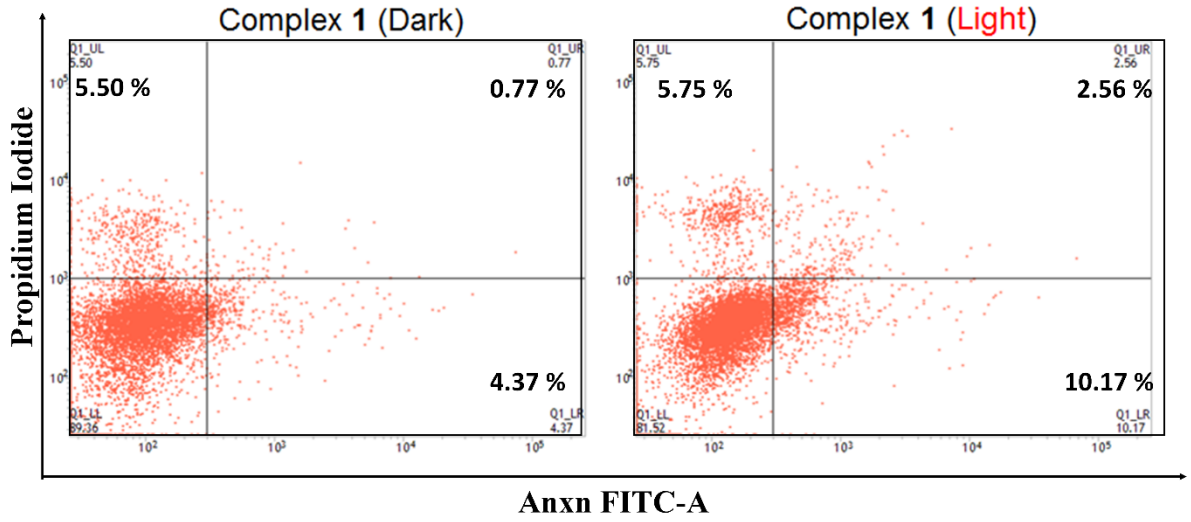

Figure S58: Annexin V-FITC/PI coupled to flow cytometry analysis showing apoptosis induced by complex 1 (5 μM) in the presence of dark and visible light (400–700 nm, 10 J cm^{-2}).

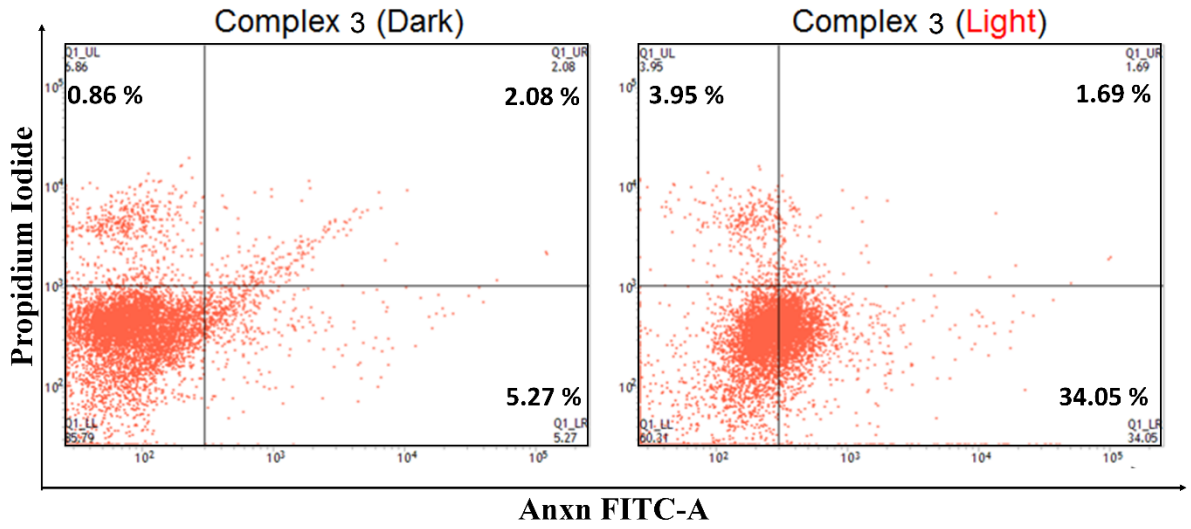

Figure S59: Annexin V-FITC/PI coupled to flow cytometry analysis showing apoptosis induced by complex 3 (5 μM) in the presence of dark and visible light (400–700 nm, 10 J cm^{-2}).